The present work was submitted to the Chair of Physical Geography and Geoecology

Of the Department of Geography, Faculty of Georesources and Materials Engineering in collaboration with the Remote Sensing Technology Institute of the German Aerospace Center

MASTER THESIS

Development of cloud-native and scalable algorithms to estimate seagrass composition and related carbon stocks in support of the Nationally Determined Contributions of the Paris Agreement

---

For the Achievement of the Academic Title

Master of Science

Within the Degree Course

Applied Geography

Submitted By

Alina Blume

Student ID 333325

First Supervisor: Dr. Georg Stauch

Second Supervisor: Dr. Dimosthenis Traganos

Aachen, 21st of September 2021

Zentrales Prüfungsamt/Central Examination Office

Eidesstattliche Versicherung
Statutory Declaration in Lieu of an Oath

Blume, Alina — 333325

Name, Vorname/Last Name, First Name — Matrikelnummer (freiwillige Angabe) / Matriculation No. (optional)

Ich versichere hiermit an Eides Statt, dass ich die vorliegende Arbeit/Bachelorarbeit/ Masterarbeit* mit dem Titel

I hereby declare in lieu of an oath that I have completed the present paper/Bachelor thesis/Master thesis* entitled

Development of cloud-native and scalable algorithms to estimate seagrass composition and related carbon stocks in support of the Nationally Determined Contributions of the Paris Agreement

selbstständig und ohne unzulässige fremde Hilfe (insbes. akademisches Ghostwriting) erbracht habe. Ich habe keine anderen als die angegebenen Quellen und Hilfsmittel benutzt. Für den Fall, dass die Arbeit zusätzlich auf einem Datenträger eingereicht wird, erkläre ich, dass die schriftliche und die elektronische Form vollständig übereinstimmen. Die Arbeit hat in gleicher oder ähnlicher Form noch keiner Prüfungsbehörde vorgelegen.

independently and without illegitimate assistance from third parties (such as academic ghostwriters). I have used no other than the specified sources and aids. In case that the thesis is additionally submitted in an electronic format, I declare that the written and electronic versions are fully identical. The thesis has not been submitted to any examination body in this, or similar, form.

Ort, Datum/City, Date — Unterschrift/Signature

*Nichtzutreffendes bitte streichen

*Please delete as appropriate

Belehrung:
Official Notification:

§ 156 StGB: Falsche Versicherung an Eides Statt
Wer vor einer zur Abnahme einer Versicherung an Eides Statt zuständigen Behörde eine solche Versicherung falsch abgibt oder unter Berufung auf eine solche Versicherung falsch aussagt, wird mit Freiheitsstrafe bis zu drei Jahren oder mit Geldstrafe bestraft.

Para. 156 StGB (German Criminal Code): False Statutory Declarations
Whoever before a public authority competent to administer statutory declarations falsely makes such a declaration or falsely testifies while referring to such a declaration shall be liable to imprisonment not exceeding three years or a fine.

§ 161 StGB: Fahrlässiger Falscheid; fahrlässige falsche Versicherung an Eides Statt
(1) Wenn eine der in den §§ 154 bis 156 bezeichneten Handlungen aus Fahrlässigkeit begangen worden ist, so tritt Freiheitsstrafe bis zu einem Jahr oder Geldstrafe ein.
(2) Straflosigkeit tritt ein, wenn der Täter die falsche Angabe rechtzeitig berichtigt. Die Vorschriften des § 158 Abs. 2 und 3 gelten entsprechend.

Para. 161 StGB (German Criminal Code): False Statutory Declarations Due to Negligence
(1) If a person commits one of the offences listed in sections 154 through 156 negligently the penalty shall be imprisonment not exceeding one year or a fine.
(2) The offender shall be exempt from liability if he or she corrects their false testimony in time. The provisions of section 158 (2) and (3) shall apply accordingly.

Die vorstehende Belehrung habe ich zur Kenntnis genommen:
I have read and understood the above official notification:

Ort, Datum/City, Date — Unterschrift/Signature

Abstract

Seagrasses are one of the world's most productive ecosystems, playing an important role in climate change mitigation and adaptation. They are vast natural carbon sinks which have important, yet largely overlooked and underestimated implications into national climate agendas like the Nationally Determined Contributions of the Paris Agreement. Precise knowledge of spatially-explicit seagrass distribution and country-specific in-situ blue carbon data is crucial for the ten countries which currently recognise this ecosystem within their Nationally Determined Contributions. This thesis combines open Sentinel-2 multi-temporal data with the open cloud computing platform Google Earth Engine to quantify country-scale seagrass extents and associated carbon stocks. The limited availability of reference data restricted the implementation of the created cloud-native mapping approach to only one country - The Bahamas. The mapped Bahamian seagrass covers an area between 11,779.44 and 27,629.32 km^2, which can store 181,610,083.57 to 455,509,862.63 Mg carbon, and sequesters between 31.02 and 72.75 Mt CO_2 per year. This equals 17 to 40 times the amount of CO_2 emitted by The Bahamas in 2018, causing a carbon-neutral state and underlining the importance of the seagrass ecosystem for the Bahamian Nationally Determined Contributions. The generated data inventories could support interdisciplinary scientific research and management efforts within a regional and global climate action context.

Contents

1 Introduction

This introduction will present the relevance of this thesis, its scope and define the research objectives.

1.1 Motivation

Climate change affects and alters the world's natural system causing an increase in extreme weather events, and the rise of ocean and land surface temperatures. In the years 2011 to 2020 the average global land surface temperature was 1.59°C higher than in the years 1850 to 1900, and the temperature over the ocean 0.88°C. These changes have been brought about by the increase in greenhouse gas emissions over the last decades (IPCC, 2021). One driver is the emission of CO_2 through the human use of fossil fuels, which increased by 47% since 1750 (Siikamäki et al., 2013; IPCC, 2021). Therefore, the United Nations Framework Convention on Climate Change (UNFCCC) adopted the Paris Agreement with the aim to limit the global average temperature rise to ideally below 1.5°C above pre-industrial levels (UNFCCC, 2016). In order to reach this goal, member countries put forward self-defined plans on climate change mitigation and adaptation actions referred to as Nationally Determined Contributions (NDCs) (UNFCCC, n.d.c). These plans comprise of a variety of strategies, including the utilisation of nature-based solutions like the carbon storage potential of coastal ecosystems (Seddon et al., 2020). One of these ecosystems is the seagrass habitat, which occupies only 0.2% of the ocean floor but can sequester up to 10% of the annual oceanic carbon burial (Duarte et al., 2005; Fourqurean et al., 2012). Since 1990, this ecosystem has been degrading at an annual rate of 7% (Waycott et al., 2009; Fourqurean et al., 2012). Even though the inclusion of seagrass meadows into NDCs can support the achievement of climate change targets of several countries, it is only recognised by a few (UNEP, 2020b). Country-scale seagrass extents, related carbon stocks and sequestration rates are necessary to assess the country-specific importance of this ecosystem (McKenzie et al., 2020). Moreover, these data inventories can support protection and restoration efforts (Roelfsema et al., 2014). The use of common time-consuming and expensive field surveying methods combined with the vast global distribution of seagrass results in large data gaps, particularly in less-developed countries. Therefore, satellite remote sensing provides a good alternative to map these vast and commonly remote areas. However, current approaches for seagrass remote sensing often lack the needed spatial resolution or quality of imagery (Veettil et al., 2020).

1.2 Objectives

In order to minimise the aforementioned data gap and to enhance the state of seagrass remote sensing, this thesis aims to develop scalable algorithms for seagrass extent and carbon inventory mapping for the ten countries which recognised this ecosystem within their NDCs. These algorithms will be developed in the cloud computing platform Google Earth Engine (GEE), will utilise high-resolution multi-temporal Sentinel-2 archives, and combine the generated maps with country-specific carbon in-situ data. The overall goal of this thesis can be divided into the following sub-objectives:

1. The design of cloud native algorithms for Sentinel-2 image pre-processing.
2. The implementation of machine learning frameworks for seagrass classification.
3. The generation of country specific seagrass carbon stock and sequestration potential ranges.
4. The evaluation of the scalability of objective 1 and 2.
5. The evaluation of the importance of the generated data for the Nationally Determined Contributions.

2 Literature Review

The following chapters will provide detailed information on the seagrass ecosystem, its related carbon stocks and its implications into the Paris Agreement. Moreover, the principles of aquatic remote sensing, Sentinel-2 and GEE will be covered.

2.1 Seagrass

Seagrasses are marine flowering plants which consist of about 72 species, six families, and twelve genera (Short et al., 2011; den Hartog and Kuo, 2006). These angiosperms can form vast intertidal and subtidal meadows with a submarine pollination mechanism allowing for reproduction, whereas the ability to perform photosynthesis favours the plants growth (Green and Short, 2003). Rhizomes and roots serve as an anchoring system to secure the plant from being displaced by strong water currents (Green and Short, 2003; Short et al., 2007). Its leaves vary greatly between species and can range from small rounded ones of 2 to 3 cm to strap-like blades of more than 4 m (Green and Short, 2003). Seagrass is often confused with algae due to its appearance but can be easily distinguished by the algal absence of seeds, flowers, and rooting system (Figure 1) (Seagrasswatch, 2021).

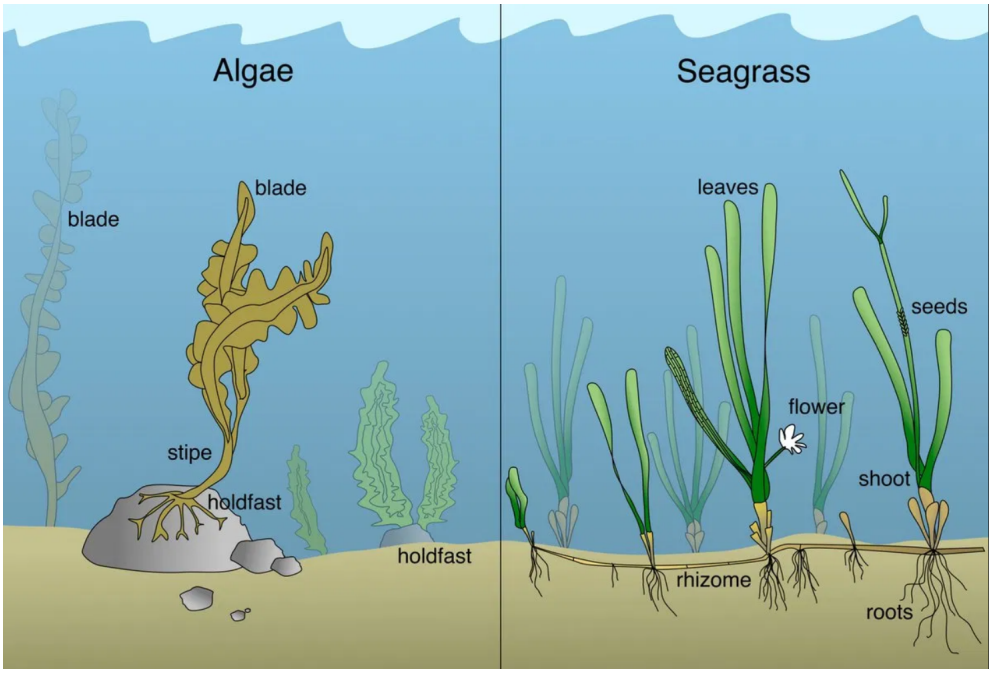

Figure 1: Physiology of algae and seagrass (Seagrasswatch, 2021).

2.1.1 Distribution

The seagrass biome is one of the most widespread coastal habitats and can be found in at least 157 countries across all continents except Antarctica (UNEP-WCMC and Short, 2018). It covers over 300,000 km^2 of seafloor worldwide and is distributed within six geographic bioregions: the Temperate North Atlantic (from North Carolina, USA to Portugal), the Tropical Atlantic (both tropical coasts of the Atlantic, the Caribbean Sea, Gulf of Mexico, Bermuda and The Bahamas), the Mediterranean (the Mediterranean, Black, Caspian and Aral Seas, and northwest Africa), the Temperate North Pacific (from Korea to Baja, Mexico), the Tropical Indo-Pacific (East Africa, South Asia, tropical Australia and the Eastern Pacific), and the Temperate Southern Oceans (New Zealand, temperate Australia, South America and South Africa) (UNEP-WCMC and Short, 2021; Short et al., 2007) (Figure 2).

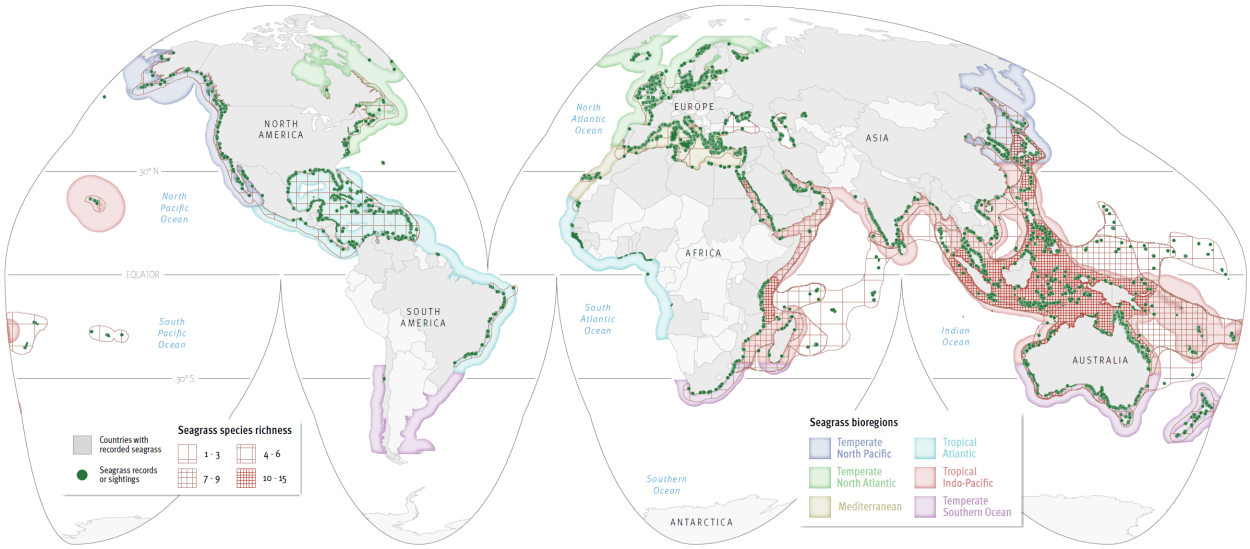

Figure 2: Global map of seagrass distribution, species richness and bioregions (Short et al., 2007; UNEP-WCMC and Short, 2018; UNEP, 2020a).

Saline conditions and light availability are essential for the plants growth and limit its living environment to shallow waters between mean sea level and 90 m of depth (Duarte, 1991). This causes seagrass to occur mainly in estuaries, lagoons and on shallow banks, where the minimum light requirements of 2 to 3% surface irradiance can be met (Short et al., 2007; Lee et al., 2007). While these plants generally grow best at salinities of 35‰, some species can tolerate ranges between 4 and 65‰, which enables them to survive in brackish and hypersaline waters (Waycott et al., 2009; Hemminga and Duarte, 2000). Another reason for their vast distribution is their ability to tolerate

temperature ranges from 0 to 45°C while withstanding water temperature variations of more than 20°C. Temperate species have their optimal growth temperature between 11.5 and 26°C, whereas tropical and subtropical species favour temperatures ranging from 23 to 32°C (Lee et al., 2007). Other factors influencing the distribution of seagrass are turbidity, nutrients, oxygen, sulphides and water currents (Veettil et al., 2020). The close proximity in which most seagrass meadows grow to other coastal habitats like mangroves, coral reefs, tidal marshes, and kelp forests is the cause for these ecosystems to be interconnected and interdependent (UNEP, 2020b).

2.1.2 Ecosystem Services

Marine ecosystems provide a number of benefits, so called 'ecosystem services', to humans and their well-being worldwide, but especially to the nearly 2.4 billion (about 40% of the world's population) living within 100 km of the coasts (United Nations, 2017; UNEP, 2006). These ecosystem services can be further categorised into the following groups: provision services such as food supply; regulation services such as climate regulation; cultural services such as tourism; and supporting services such as soil formation and habitat provision, which are necessary for the production of all other services. All service groups are interconnected and supported by the preservation of biodiversity (UNEP, 2006).

Covering about 46% of the global area of marine ecosystems (seagrass, mangroves, and coral), seagrass has a high impact on human and animal well-being by providing a wide range of services (UNEP, 2020b). The almost constantly submerged and complex three-dimensional structure of seagrass meadows provides shelter for many fish and invertebrates throughout the tidal cycle, while also being the food source of animals like dugongs, manatees, sea turtles, and waterfowls (Waycott et al., 2011; Green and Short, 2003). These meadows therefore support the fishing industry by serving as nursing habitats for over 20% of the world's 25 largest fisheries (Unsworth et al., 2019). Thus, seagrass ecosystems are important for seafood supply which represents the main source of animal protein for about 17% of the global population and more than half in many least-developed countries (United Nations, 2017). Another seagrass service is water quality improvement through filtration and uptake of nutrients and pollutants, as well as human, fish and coral disease control through pathogens removal (UNEP, 2020a). Climate change induced sea level rise, flooding, and land erosion affects about 100 million people living in coastal areas who benefit from healthy seagrass (Twomey et al., 2020). Their submerged canopies can minimise these impacts by

reducing water flow and wave energy by 40% per metre of seagrass bed, while also stabilising the sediment through their roots (Fonseca and Cahalan, 1992; Cullen-Unsworth and Unsworth, 2013). This stabilisation combined with their ability to trap sediments can cause seabed elevation at a rate of 31 mm per year and therefore contributes to the adaptation to sea level rise (Potouroglou et al., 2017). Moreover, seagrass meadows play an important role in climate change mitigation as they represent significant carbon sinks which are estimated to sequester 27.4 Tg carbon per year (Fourqurean et al., 2012) (Chapter 2.2). This uptake of carbon through photosynthesis can increase seawater pH and create potential acidification refugia for nearby calcifying organisms like corals (Manzello et al., 2012). Furthermore, seagrass areas are of religious and spiritual importance, and create touristic, recreational and educational opportunities (UNEP, 2020a). The total economic value of these ecosystem services is estimated to be US $3,400,000 per km^2 per year (Short et al., 2011).

2.1.3 Threats

Marine habitats face a number of land-, sea-, and climate-based threats causing their global deterioration (UNEP, 2020a). Since 1990, seagrass areas have been declining at a rate of approximately 7% per year with a total habitat loss of 29% since 1879 (Waycott et al., 2009). Human activities such as boating, trawling, and coastal development can cause the direct displacement of seagrass meadows, while the input of contaminants from urban and agricultural run-off slowly alters seagrass health (Grech et al., 2012). Climate change intensified rainfall events increase the amount of pollutants and sediment load which enter the oceans and can therefore reduce light availability for marine habitats. In areas with long water resident times, like lagoons and bays, strong rainfall events can also reduce sea surface salinity and hinder seagrass growth (Waycott et al., 2011). Another threat these plants are facing is sea level rise, which causes light availability reduction and therefore seagrass migration to shallower areas. This migration could be inhibited by the presence of impervious surfaces like anthropogenic structures and cause the loss of habitat area (Saunders et al., 2013). Despite their general tolerance to wide ranges of sea surface temperatures (Chapter 2.1.1), a temperature increase can lead to ecosystem degradation since many seagrass meadows are already growing at their maximum temperature tolerance (Waycott et al., 2011). Even though these threats and the consequences regarding seagrass habitat loss are well researched, only 16% of its area currently lies within marine protected areas (MPAs) (UNEP, 2020a).

2.2 Blue Carbon

Blue carbon describes the carbon stored in vegetated coastal ecosystems such as salt marshes, mangroves, macroalgae, and seagrass meadows (Duarte et al., 2013b). Despite only covering 0.2% of the ocean floor, seagrass meadows account for nearly 10% of the oceanic yearly carbon burial with carbon sequestration rates 35 times faster than tropical rainforests (Duarte et al., 2013a; Fourqurean et al., 2012; Macreadie et al., 2015; Mcleod et al., 2011). This carbon (C) is stored in the above-ground biomass (AGB) (leaves and stems), the below-ground biomass (BGB) (roots and rhizomes), and the underlying sediment (Macreadie et al., 2014; Bandeira, 1997):

$$C_{total} = C_{AGB} + C_{BGB} + C_{soil} \tag{1}$$

Total living biomass carbon has a global average of 252±48 Mg carbon per km^2, two-thirds of it being C_{BGB}, and one-third being C_{AGB} (Figure 3) (Fourqurean et al., 2012). An increase in the below- to above-ground biomass ratio causes a rise of total seagrass carbon (Brodie et al., 2020) (Figure 4). Parts of this carbon can be exported from the meadows through animal grazers (Valentine and Heck, 1999). The amount of carbon contained in the top metre of sediment features a global average of 19,420±2,020 Mg carbon per km^2, exceeding those of non-vegetated marine sediments by two to tenfold, and those of terrestrial forests by 30 to 50 fold (Fourqurean et al., 2012; Duarte et al., 2005, 2013b; Mcleod et al., 2011). This carbon can be sustained for millennia due to low soil oxygen levels, slow composition rates, and vertical sediment accretion which causes marine soil to not become saturated with carbon (Macreadie et al., 2012; Duarte et al., 2013b; Mcleod et al., 2011). About 50% of seagrass sediment carbon is estimated to be allochthonous due to the constant exchange between marine ecosystems through currents, tides, and waves (Kennedy et al., 2010; Santos et al., 2021). Both biomass and sediment carbon are dependent on light availability and decrease with water depth (Duarte, 1991; Serrano et al., 2014). The species *P. sinuosa*, for instance, shows a fourfold decrease in organic carbon in the top metre of sediment from 2 to 4 m to 6 to 8 m water depth, while *P. oceanica* meadows show a fourteen- to sixteenfold decrease from 2 to 32 m (Serrano et al., 2014). Additionally, carbon content decreases with sediment depth since it is closely linked to the presence of roots (Fourqurean et al., 2012; Brodie et al., 2020). Other factors influencing total seagrass blue carbon storage are bioturbation, nutrient input, soil oxygen content, and species composition (Brodie et al., 2020). Global blue carbon stocks per seagrass meadow area range from 1,000 to 829,000 Mg carbon per km^2, with a mean of 108,000 Mg carbon per km^2 which is comparable to 396,000 Mg carbon dioxide (CO_2)

equivalents per km^2 (The Blue Carbon Initiative, 2014). Globally, the seagrass ecosystem could store between 4.2 and 8.4 Pg carbon (Fourqurean et al., 2012).

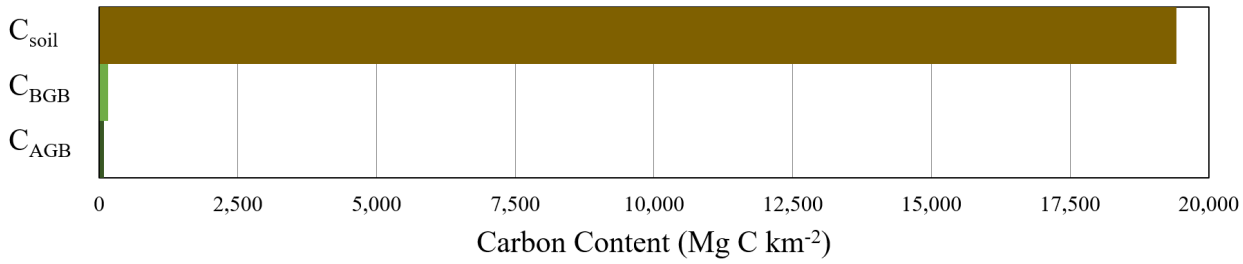

Figure 3: Ratio of soil (C_{soil}), below-ground (C_{BGB}), and above-ground carbon (C_{AGB}) in Mg C km^{-2} (Adapted from Fourqurean et al., 2012).

Taking current habitat loss rates into account, a sequestration potential loss of 6 to 24 Tg carbon per year and a release of 0.15 to 1.02 Pg CO_2 per year is estimated, shifting seagrasses from carbon sinks to carbon sources (Fourqurean et al., 2012; Pendleton et al., 2012; Macreadie et al., 2014). This release of carbon is equivalent to economic damages of 6 to 42 billion USD annually (Pendleton et al., 2012).

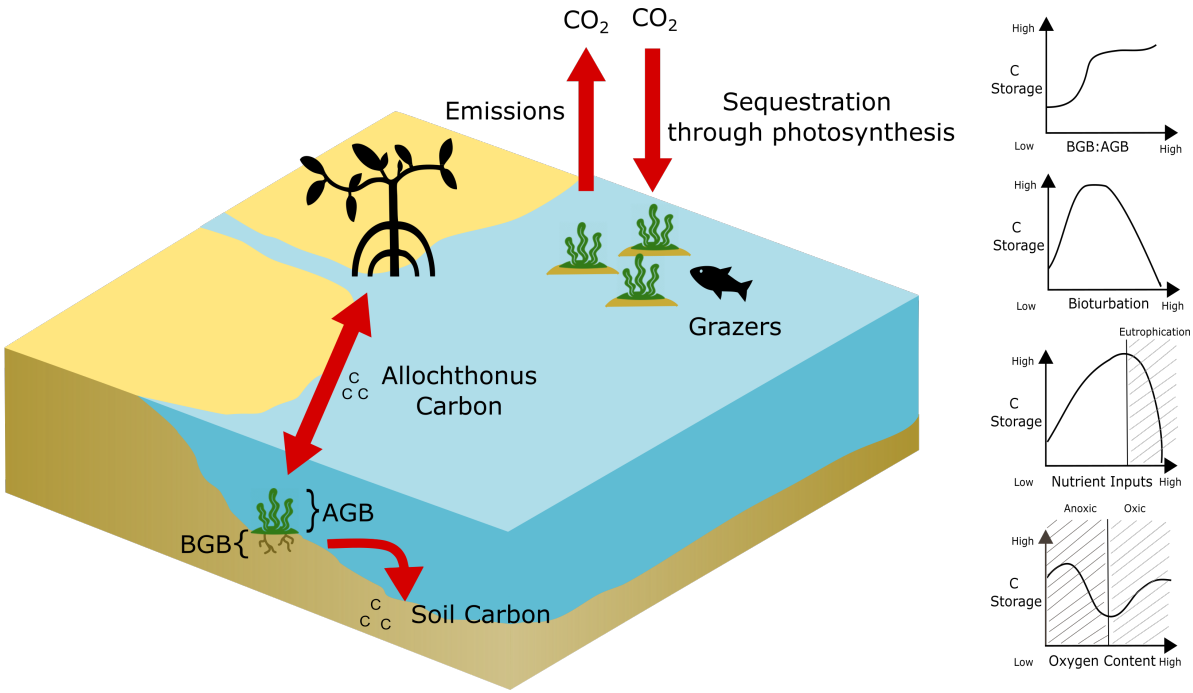

Figure 4: Model of a seagrass blue carbon ecosystem and sediment depth independent relationships between seagrass carbon storage, and physical and biological parameters. AGB denotes above-ground biomass, BGB denotes below-ground biomass, and C donates organic carbon (Adapted from The Blue Carbon Initiative, 2014; Brodie et al., 2020).

2.3 Paris Agreement

The Paris Agreement's aim is to reinforce actions on climate change mitigation by limiting the global average temperature rise for the twenty-first century to below 2°C, ideally below 1.5°C, above pre-industrial levels (UNFCCC, 2016). It was adopted on the 12th of December 2015 at the twenty-first session of the Conference of the Parties to the UNFCCC and the eleventh session of the Kyoto Protocol (UNFCCC, n.d.b,n). The agreement was signed by 191 countries and entered into force on the 4th of November 2016 (UNFCCC, n.d.d). To reach this long-term goal the NDCs were established (UNFCCC, 2016). These NDCs require each country to put forward self-defined measures on how to achieve emission reduction and adaptation to climate change impacts (UNFCCC, n.d.c). Moreover, countries are required to regularly report on their implementation efforts and emissions. In support of the member states, especially developing and least-developed countries, the agreement provides enhanced capacity-building, financial resources, and a technology framework (UNFCCC, n.d.b). To determine the progress of these set efforts each country is obligated to communicate their revised NDCs every five years (UNFCCC, n.d.b, 2016). Each successive NDC must demonstrate improved measures and represent the highest possible ambition (UNFCCC, 2016).

Coastal blue carbon ecosystems are vast natural carbon sinks and therefore contribute to national carbon stock inventories in support of the Paris Agreement's main goal of climate change mitigation and adaptation. These ecosystems are being recognised in the NDCs of several countries. Sixty-four out of the 185 countries which submitted their NDCs by 2019 mentioned marine and coastal ecosystems regarding their climate change adaptation and mitigation abilities, although only ten recognise seagrass specifically. Eight of these mention seagrass in terms of adaptation and five with a reference to mitigation. Only one country, The Bahamas, has set a measurable target of protecting 20% of the nearshore marine environment by 2020 (UNEP, 2020a; The Government of the Bahamas, 2015).

2.4 Coastal Aquatic Remote Sensing

Precise knowledge of seagrass' spatial extent is necessary to estimate their impact on country-scale carbon stock inventories and therefore on the requirements of the Paris Agreement (McKenzie et al., 2020). Remote sensing provides a less time-consuming and inexpensive alternative to traditional land- or boat-based surveying methods, especially for remote areas (Hossain et al., 2015; Veettil et al., 2020). Commonly used space- and airborne remote sensing data include hyperspectral and multispectral optical imagery, and Light Detection and Ranging (LiDAR) measurements (Li et al., 2012; Phinn et al., 2008; Pan et al., 2016). Current satellite-based approaches for seagrass mapping feature spatial resolutions of 0.30 to 30 m, temporal resolutions of one to 17 days, spectral bands of the visible spectrum between 400 and 700 nm, and infrared radiation between 1,000 and 2,000 nm (UNEP, 2020a; Veettil et al., 2020).

The aquatic nature of seagrass requires additional processing of satellite data compared to the conventional terrestrial remote sensing. This is based on the fact that the path of light is influenced by water as an additional medium to air (Roelfsema et al., 2013). When light reaches the water surface, it either penetrates into it or is reflected back into the atmosphere (Phinn et al., 2018). In the case that sunlight is directly reflected towards the sensor as a function of sun position and sensor viewing angle in relation to the water, a light pollution effect called sunglint can occur (Kay et al., 2009; Phinn et al., 2018). This effect can be either limited to waves at certain viewing angles, or cover large parts of an image (Phinn et al., 2018). Radiation gets refracted and partly attenuated as it penetrates the air-water interface, and while travelling towards the bottom (downwelling) and back to the water surface (upwelling) (Kirk, 1977; Lee et al., 1999). This attenuation is a result of the presence of suspended sediments and phytoplankton in the water column, which cause spectral scattering and absorption. These effects increase with water depth and turbidity, and cause an exponential reduction in light intensity (Veettil et al., 2020; Phinn et al., 2018). Absorption, and therefore attenuation, affects longer wavelengths stronger, rendering the visible spectral range the most suitable for seagrass detection (Åhlén et al., 2003; Veettil et al., 2020). Within the visible range, mainly blue and green bands are used for the differentiation of shallow water bottom features, because the light sensed by the red band is completely absorbed at a depth of about 3 m (Åhlén et al., 2003). In optically deep waters, all radiation is absorbed before reaching the seabed, leaving no bottom signal to be returned to the sensor (Phinn et al., 2018).

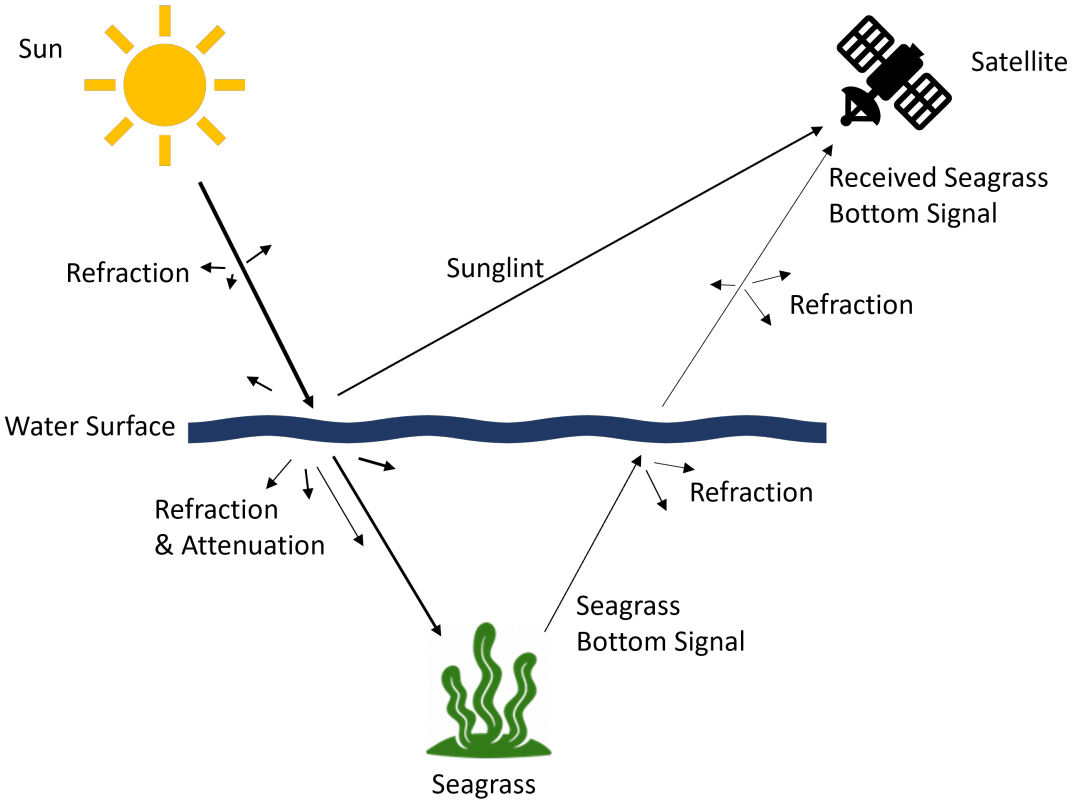

Figure 5: Schematic model of coastal aquatic remote sensing (Adapted from Komatsu et al., 2020).

Phinn et al. (2018) concludes that seagrass meadows cannot be detected by airborne or satellite remote sensing if water clarity is strongly reduced by dissolved or suspended material, in clear waters of more than 15 m depth, or if the meadows have densities lower than 20%.

2.5 Sentinel-2

Sentinel-2 is a multi-spectral imaging mission within the Copernicus programme of the European Space Agency (ESA). The mission aims to monitor earth's surface changes and consists of two sun-synchronous, identical satellites named Sentinel-2A and Sentinel-2B (ESA, 2015). Sentinel-2A was launched on the 23rd of June 2015, and Sentinel-2B on the 7th of March 2017 (ESA, 2020). The satellites are phased at 180° to each other, causing a revisit frequency of five days at the Equator. Both satellites have a swath width of 290 km, and cover land and coastal areas between 56° South and 83° North. They passively collect data of all European islands, the Mediterranean Sea, all world islands greater than 100 km^2, all waters within 20 km of the shore, and all closed seas. The satellites are equipped to sample thirteen spectral bands, four at 10 m, six at 20 m, and three at 60 m spatial resolution. User products are released as Level-1 (Top-of-Atmosphere) and Level-2 (Bottom-of-Atmosphere) products (ESA, 2015).

Seagrass habitat mapping requires satellite imagery to have a finer resolution than the habitat's dimensions in order to minimise mixed pixel creation. Meadows generally have a horizontal scale between several metres to thousands of metres (Komatsu et al., 2020). Sentinel-2's high spatial and temporal resolution, its coverage of coastal areas, and ESA's free and open data policy qualify this mission as suitable for seagrass mapping (Traganos and Reinartz, 2018c).

2.6 Google Earth Engine

GEE is a cloud computing platform which combines multi-petabyte analysis-ready data with a high-performance, parallel computation service allowing for rapid multi-image processing and analysis (Gorelick et al., 2017; Traganos et al., 2018b). It follows the client-server programming model in which scripting and computationally light operations are performed in the local programming environment (client side/browser) while computationally heavier processes are executed by Google's cloud server (server side) (Gorelick et al., 2017; Navarro, 2017). The integrated geospatial data repository consists of a large number of freely available datasets, including satellite and aerial imagery, environmental variables, and climate forecasts. Additionally, users can integrate and process their own datasets. GEE offers the usage of JavaScript and Python as scripting languages, as well as more than 800 internal functions. These range from simple mathematical functions to complex and powerful image processing operations. Rapid scripting and result visualisation are supported through a web-based interactive development environment with the possibility to examine results by panning and zooming. Moreover, GEE provides a wide range of machine-learning toolkits for supervised and unsupervised classification, regression, and confusion matrices for accuracy assessment. Its web-based nature allows for an easy sharing of user generated datasets and scripts (Gorelick et al., 2017).

The computational power of GEE has been used for a variety of data-heavy, aquatic remote sensing projects like coral reef, tidal flat and surface water mapping, as well as satellite-derived bathymetry estimation (Lyons et al., 2020; Murray et al., 2019; Donchyts et al., 2016; Traganos et al., 2018b). Previously, it has also been implemented for large-scale seagrass mapping in the work of Traganos et al. (2018a).

3 Methodology

The following methodology documentation covers the chosen study areas, the auxiliary data acquisition, the image pre-processing procedure, the seagrass classification frameworks, and the calculation of related carbon stocks and sequestration potentials.

3.1 Study Area

The ten countries which recognise seagrass within their NDCs are The Bahamas, The Kingdom of Bahrain, Honduras, Kiribati, Mauritius, Mexico, Saint Kitts and Nevis, Sri Lanka, Sudan, and The United Arab Emirates (Figure 6). Three of these, The Bahamas, Mexico, and The United Arab Emirates, have included seagrass in both their mitigation and adaptation actions. Honduras, Mauritius, Saint Kitts and Nevis, Sri Lanka, and Sudan only focus on adaptation actions, while The Kingdom of Bahrain and Kiribati merely target mitigation (UNEP, 2020a).

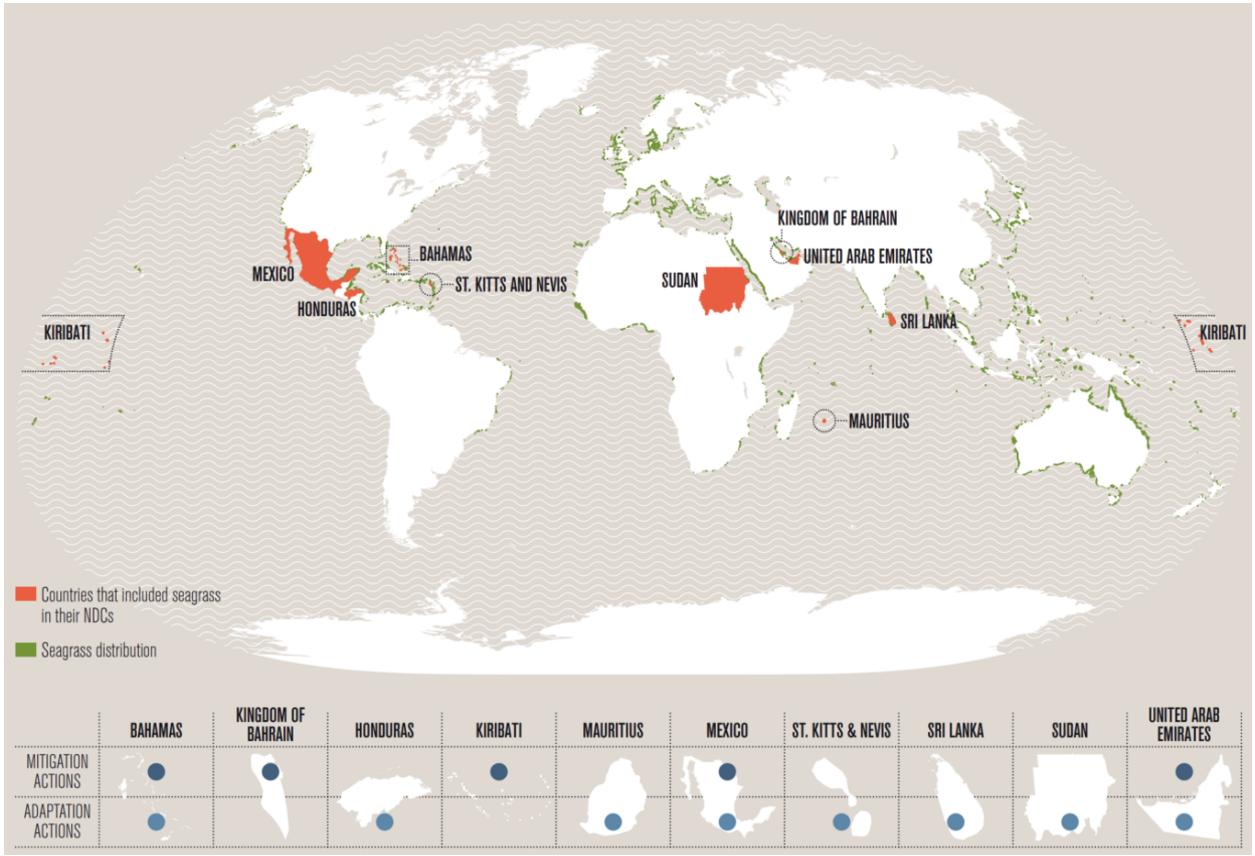

Figure 6: Map of countries with a specific reference to seagrass within their Nationally Determined Contributions, world-wide seagrass distribution, and table of actions taken by countries (UNEP, 2020a)

The study area stretches over three bioregions (Tropical Atlantic, Tropical Indo-Pacific, and Temperate North Pacific) and covers a total area of 9,398,913 km^2 (Table 1) (Short et al., 2007; Flanders Marine Institute, 2019). Seventeen species can be found in this region: *Cymodocea serrulata, Enhalus acoroides, Halodule uninervis, Halodule wrightii, Halophila beccarii, Halophila decipiens, Halophila engelmanni, Halophila ovalis, Halophila stipulacea, Phyllospadix scouleri, Phyllospadix torreyi, Syringodium filiforme, Syringodium isoetifolium, Thalassia hemprichii, Thalassia testudinum, Thalassodendron ciliatum*, and *Zoestra marina*. Kiribati represents the country with the lowest biodiversity with only one species, while Mexico shows the highest biodiversity with seven different species (Green and Short, 2003). It also has the longest coastline at 9,330 km. The country with the shortest coastline is The Kingdom of Bahrain (ChartsBin, 2010).

Country	BHS	BHR	HND	SDN	LKA	KNA	ARE	MUS	MEX	KIR
EEZ [km^2]	619,785	7,516	208,636	62,82	533,559	9,502	51,674	1,278,182	3,187,013	3,440,220
CL [km]	3,542	161	820	853	1,340	135	1,318	177	9,330	1,143
Bio-region	TA	TIP	TA	TIP	TIP	TA	TIP	TIP	TNP/TA	TIP
No. of Sp.	3	3	2	7	7	2	3	7	8	1

Table 1: Summary of country-specific Exclusive Economic Zone (EEZ) areas in km^2, coastline length (CL) in km, associated bioregion, and number of species (No. of Sp.) (Flanders Marine Institute, 2019; ChartsBin, 2010; Short et al., 2007; Green and Short, 2003). Country names are represented as ISO 3166 Alpha-3 codes: BHS = The Bahamas, BHR = Kingdom of Bahrain, HND = Honduras, SDN = Sudan, LKA = Sri Lanka, KNA = Saint Kitts and Nevis, ARE = United Arab Emirates, MUS = Mauritius, MEX = Mexico, KIR = Kiribati. Bioregion abbreviations denote: TA = Tropical Atlantic, TIP = Tropical Indo-Pacific, TNP = Temperate North Pacific.

3.2 Auxiliary Data Acquisition

The following chapters describe the acquisition of in-situ carbon data and country-scale carbon emissions, as well as the methodology used to calculate country-specific carbon stock and sequestration potential ranges.

3.2.1 In-situ Data Collection

A systematic technical review was implemented to collect country-scale seagrass blue carbon data. For this, Google Scholar, and the reference lists of related articles were used to identify relevant literature regarding country-specific seagrass species composition, carbon inventories, carbon sequestration rates and biomass. The search was based on the following term combinations: [(country OR bioregion) + ('seagrass' OR more precise species)] OR [(country OR bioregion) + ('seagrass' OR more precise species) + ('carbon' OR 'sequestration' OR 'biomass' OR 'blue carbon' OR 'soil carbon'). Articles were then screened for in-situ biomass and carbon data in the form of species- or region-specific ranges. Therefore, literature which only stated averaged numbers for biomass or carbon stocks were excluded.

3.2.2 Areal Carbon Stock Range Calculation

In order to calculate total carbon inventory ranges for each target country (Section 3.5), the literature review based in-situ data was harmonised. For this, the country-level average minimum and maximum carbon content was calculated. If no country-specific data was available, bioregional averages were used.

First, the range for biomass carbon was estimated. Dry weight biomass was converted to biomass carbon following Fourqurean et al. (2012):

$$Biomass\ Carbon = 35\%\ Dry\ Weight\ Biomass \tag{2}$$

In the case that both dry weight biomass and biomass carbon were stated, the latter was chosen. Total biomass (TB), AGB, and BGB were calculated as follows (Fourqurean et al., 2012):

$$\begin{aligned} TB &= AGB + BGB \\ AGB &= \frac{1}{3} * TB = \frac{1}{2} * BG \\ BGB &= \frac{2}{3} * TB = 2 * AGB \end{aligned} \tag{3}$$

To minimise uncertainties some papers were excluded from the calculation based on the kind of data they provide. Since AGB:BGB ratios can vary significantly between species, papers which only state only one kind of biomass (AGB or BGB) were excluded when there were more than two other sources stating TB (Duarte and Chiscano, 1999). Moreover, sources which define regional AGB and BGB ranges based on different sites were excluded when there were more than two other sources of TB. This is due to the fact that different study sites do not necessarily show the same species composition and therefore self-calculated TB values are not fully representative. If a paper presents both species- and regional-level ranges, the regional ones were used.

To prevent incorrect weighting, species and regional specific ranges were created separately before calculating the final average range. The prevalence of species was taken into account if given. In the last step, carbon stock ranges in Megagrams per km^2 were created as followed:

$$\begin{aligned} C_{min} &= C_{TB_{min}} + C_{soil_{min}} \\ C_{max} &= C_{TB_{max}} + C_{soil_{max}} \end{aligned} \tag{4}$$

3.2.3 Carbon Emissions

Country-scale carbon emissions between 1960 to 2018 were derived from Friedlingstein et al. (2020). These emissions were later (Chapter 3.5) used to evaluate the seagrass carbon sink potential per country.

3.3 Image Pre-Processing

In order to achieve the best possible seagrass classification result, Sentinel-2's image archive was pre-processed and reduced to a single composite per country (Figure 7).

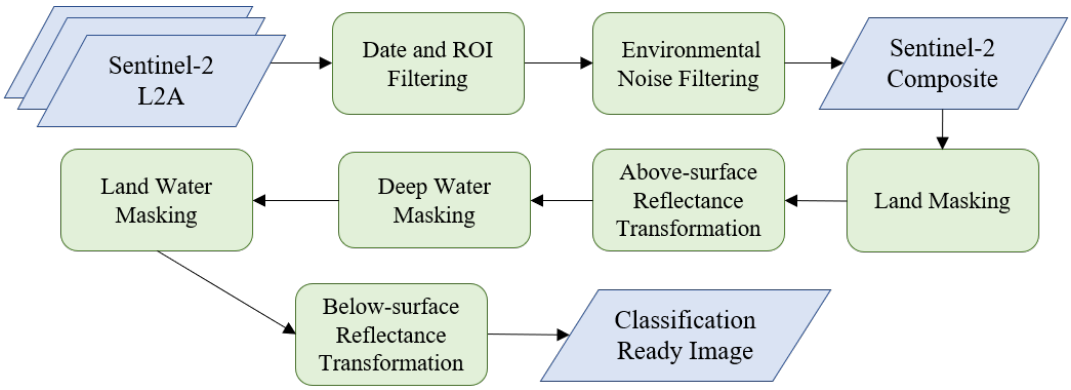

Figure 7: Schematic pre-processing workflow. Blue boxes represent image products, green boxes show used methods. L2A denotes Level 2A, and ROI denotes region of interest.

3.3.1 Sentinel-2 Imagery

The Sentinel-2 Bottom Of Atmosphere (Level 2A) image archive within GEE was utilised for the country-scale pre-processing and seagrass mapping procedure. For this, four years' worth of images, taken between the 28th of March 2017 and the 28th of March 2021, were used (see Table 2 for image count per country). These images are orthorectified, projected in Universal Transverse Mercator (UTM)/World Geodetic System 1984 (WGS84), and were clipped to the regions of interest (ROI). ROIs cover Exclusive Economic Zones (EEZ) and nearshore landmasses. EEZs were taken from Flanders Marine Institute (2019) and processed using ArcGIS in order to keep land pixels to allow for the pixel-based land masking (Chapter 3.3.4). Non-island EEZs were manually extended to cover parts of the nearshore land. For island countries, the EEZ shape file was edited using ArcGIS' *union*-function with the option to not allow for gaps.

Country	BHS	BHR	HND	SDN	LKA	KNA	ARE	MUS	MEX	KIR
Image Count	18,881	849	12,035	4,748	9,106	1,333	6,900	3,295	71,893	26,305

Table 2: Number of Sentinel-2 Level-2A Images processed per country. Country names are represented as ISO 3166 Alpha-3 codes: BHS = The Bahamas, BHR = Kingdom of Bahrain, HND = Honduras, SDN = Sudan, LKA = Sri Lanka, KNA = Saint Kitts and Nevis, ARE = United Arab Emirates, MUS = Mauritius, MEX = Mexico, KIR = Kiribati.

3.3.2 Environmental Noise Filtering

The pre-filtered Sentinel-2 archive was further processed to reduce cloud and sunglint effects. First, the Red Edge 4 (20 m resolution) and Water Vapor (60 m resolution) bands were used to mask insufficient pixel values at the scene edges of every image in the collection (GEE, n.d.a). The enhanced archive was then filtered for images with a mean solar zenith angle of less than 70%. This filter value was used to allow for enough scenes to reduce sunglint effects while excluding images with possibly insufficient data due to long atmospheric paths between radiation source and sensor. For further filtering, the Sentinel-2 imagery was joined with the corresponding Cloud Probability dataset (GEE, n.d.a). This collection was filtered for images with a cloudy pixel percentage of less than 25%, and the QA60 bitmask band in 60 m resolution was used to mask out opaque and cirrus clouds in each image (GEE, n.d.b). Moreover, images were masked using Sentinel's Scene Classification Map band which contains information on cloud shadows and cirrus clouds in 20 m resolution. Additionally, the Cloud Probability dataset's probability band was utilised to mask pixels with a cloud probability of over 30%. In the last step, all pixel values were divided by 10,000 for a conversion from integers to values in the range of 0 to 1.

3.3.3 Multi-Temporal Composition

In order to create a single multi-temporal composite with reduced interference of sunglint, turbidity, waves, remaining clouds, and haze, a GEE-reducer based on the 20^{th} percentile of each pixel was used (Thomas et al., 2021). This reducer minimises high-reflectance obstacles within the image (Traganos et al., 2021).

3.3.4 Land Masking

Land pixels were identified and masked using the combined Otsu and Canny edge filter method of Donchyts et al. (2016). This method uses the Modified Normalised Difference Water Index (MNDWI) (Equation 5) as input for the Canny edge filter in order to detect pixels located near water-land edges with sharp value changes (Xu, 2006).

$$MNDWI = \frac{Green - SWIR1}{Green + SWIR1} \tag{5}$$

The lower the index value, the more likely the pixel represents land mass. Detected edges were buffered by 10 m and used for Otsu-based thresholding, which aims to decrease intra-class variance within a gray-scale histogram (Otsu, 1979).

In order to not exceed GEE's computation time, the amount of input pixels was limited by manually defined bounding boxes. For sparsely vegetated countries (Bahrain, Sudan, and United Arab Emirates) the threshold which defines the sensitivity of the Canny edge filter was set to 0.4, and the sigma value which defines the standard deviation of the Gaussian smoothing kernel was set to 0.3. The values for all other countries were set to 0.9 and 1, respectively. Additionally, the number of buckets for the Otsu-histogram was set to 100, and an Otsu-threshold minimum of 0.05 was chosen.

3.3.5 Above-Surface Reflectance Transformation

The normalised water leaving reflectance composite R_{hown} was corrected to account for the difference in the optical pathway between the air and water column. For this, the above-surface remote sensing reflectance (R_{rs}), which describes the ratio of the water leaving radiance to downwelling radiance just above the water surface, was obtained as followed (Traganos and Reinartz, 2018b):

$$R_{rs} = \frac{R_{hown}}{\pi} \tag{6}$$

Moreover, the environmental noise of optically deep water within two 32x32 pixel areas was calculated using a standard deviation reducer for the bands B2 (Blue), B3 (Green), B4 (Red), B8 (Near Infrared), and B11 (Shortwave Infrared 1). One polygon was placed close to the centre of a Sentinel-2 tile, and another one was placed at the overlapping border of two tiles. The calculated noise was then compared to the optimal value of <0.00025 sr^{-1} (Chapter 4.2.1) (Dörnhöfer et al., 2016; Giardino et al., 2015; Brando and Dekker, 2003).

3.3.6 Deep Water Masking

Optically deep waters were masked out in order to limit the classification input to areas with a possibility for seagrass growth and to avoid misclassification. These optically deep waters are defined as areas where reflectance is not affected by bottom signals, and were identified using Otsu thresholding (Traganos and Reinartz, 2018c). For this thresholding, two indices and self-defined bounding boxes were used. First, a normalised index based on Sentinel-2's band 2 (Blue) and band 3 (Green) was implemented due to their ability to penetrate deep into the water column (Traganos and Reinartz, 2018c; Alkhatlan et al., 2019):

$$Shallow\ Water\ Index = \frac{Green - Blue}{Green + Blue} \tag{7}$$

Increased water depth corresponds to an increased Shallow Water Index value since the reflectance of the green band, which has a higher absorption ability, decreases proportionately faster than the reflectance of the blue band (Stumpf et al., 2003). Moreover, the MNDWI was applied to detect optically deep water areas, which show higher values than shallow waters. Minimum threshold values were set to -0.5 for the Shallow Water Index, and to -0.3 for MNDWI. The number of buckets for both histograms was set to 100, and the use of self-defined bounding boxes allowed for a manual histogram adjustment which helped to achieve stronger bio-modal distribution.

Additionally, the National Oceanic and Atmospheric Administration's (NOAA) ETOPO1 1 Arc-Minute Global Relief Model was used to mask pixels of more than 1 km depth (NOAA National Geophysical Data Center, 2009).

The accuracy of the masking output was estimated using nautical charts and a visual ocean colour assessment. Remaining deep water pixels were masked manually following a visual examination of the image.

3.3.7 Land Water Masking

The Global Administrative Unit Layers 2015 (GAUL) dataset, implemented by the Food and Agriculture Organization of the United Nations (FAO), was manually edited and used to mask land-based water bodies (FAO UN, 2014). Polygon editing was based on visual examination of the coastline and applied to un-mask areas with possibilities for seagrass growth like salt-water lagoons and river deltas.

3.3.8 Below-Surface Reflectance Transformation

The sub-surface remote sensing reflectance (r_{rs}), which describes the ratio of the water leaving radiance to downwelling radiance just below the water surface, was derived from R_{rs} following Lee et al. (1998):

$$R_{rs} = \frac{\zeta r_{rs}}{1 - \Gamma r_{rs}} \tag{8}$$

The water-to-air radiance-divergence factor ζ was set to 0.5, and Γ within the denominator was set to 1.5 (Lee et al., 1998, 1999). The latter accounts for effects of internal reflection from water to air which can be large for shallow waters (Lee et al., 1998; Traganos and Reinartz, 2018b).

3.4 Seagrass Classification

The classification ready image generated in Chapter 3.3 is the base for the unsupervised and supervised classification approach (Figure 8). This chapter therefore also covers the input-data preparation and the accuracy assessment.

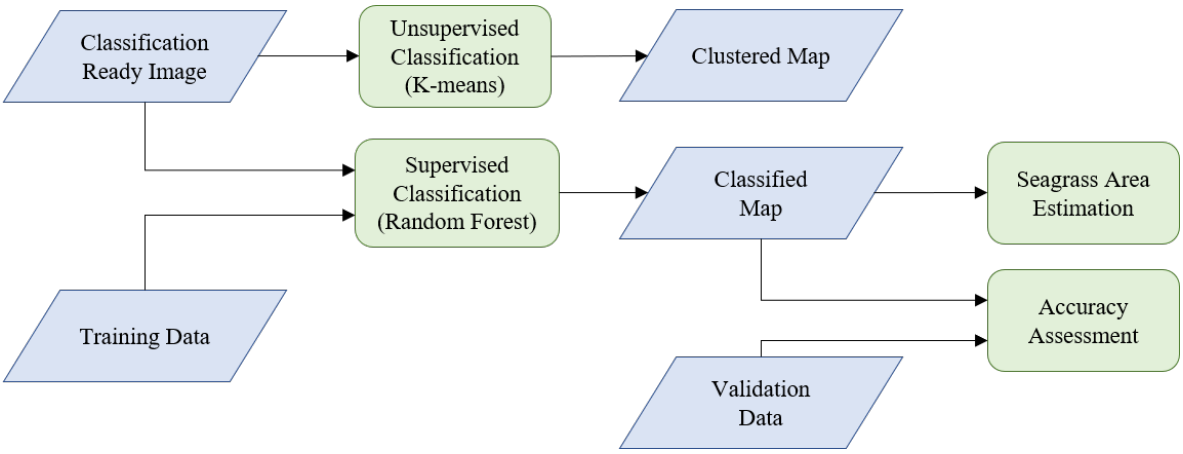

Figure 8: Schematic classification workflow. Blue boxes represent data products, green boxes show used methods.

3.4.1 Unsupervised Classification

An unsupervised classification was used to gain an understanding of possible pixel clusters and to assess the necessity for a supervised classification. For this, the K-means clustering method *ee.Clusterer.wekaKMeans()* was applied to the classification ready image within GEE. This classifier divides an image into a given number of classes based on the spectral intensities of pixel (Rekik et al., 2006). Five-thousand training points were randomly selected and used to create five discrete classes. This number of classes was based on the observed number of marine habitats in Bahamian waters by the Allen Coral Atlas (ACA) project. These classes are: Seagrass, Coral/Algae, Rock, Rubble, and Sand (Allen Coral Atlas, 2020).

3.4.2 Input-Data Preparation

The supervised classification (Section 3.4.3) was based on data provided by the ACA. This data included classified maps in raster format and ground truth data in vector format. Due to the ACA's use of PlanetScope satellite imagery with a spatial resolution of 3.125 m, a reprojection and res-

olution reduction was necessary to match the 10 m resolution of Sentinel-2 (Allen Coral Atlas, 2020). In order to do this, the vector data was converted into raster format and combined with the image pixel values beforehand. Then the *ee.Reducer.mean()* reducer was used to create pixels of lower resolution. The resolution of the classified data was resampled using the majority reducer *ee.Reducer.mode()* to allocate the most frequent class to each 10 m-pixel. This extent was then combined with the image pixel values. Both classified and ground truth data were divided into two classes: Seagrass and Non-Seagrass (merged class of Coral/Algae, Rock, Rubble, and Sand).

To account for possible misclassifications by the ACA, the classified data was harmonised with the ground truth data using Sentinel-2's spectral bands B1 to B5. For this, the minimum and maximum reflectance per class of the ground truth data was used to filter out pixels of the classified data which did not fall within this range (Figure 9). The leftover spectral ranges will be referred to as Spectral Range 1 in the following.

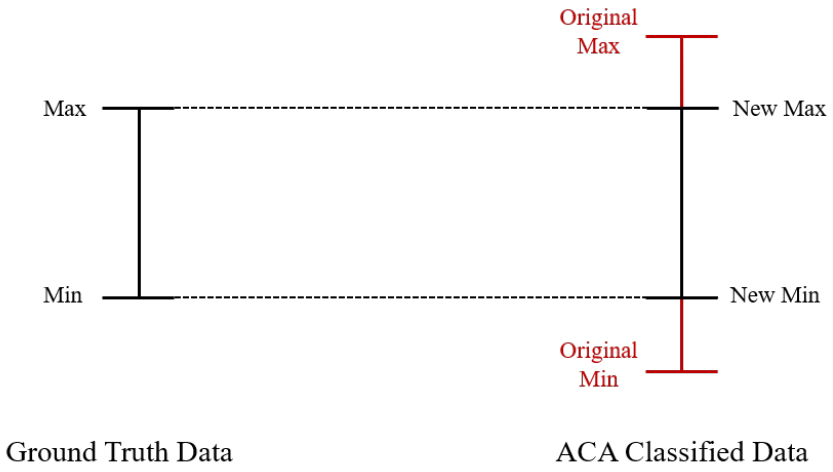

Figure 9: Harmonisation procedure for ACA's classified data with the ground truth data (Spectral Range 1). Bars show spectral ranges and red parts show pre-filtered data. Min denotes minimum and Max denotes maximum.

Moreover, a second version (Spectral Range 2) was created using the minimum and the 80th percentile of the seagrass ground truth data as a filter for itself and for classified seagrass pixels (see Figure 10). This aimed to reduce the number of high reflectance mixed pixels which could have been created by the resolution reduction and which are likely to represent a combination of the seagrass and sand habitat.

Figure 10: Harmonisation procedure for ACA's classified seagrass data with the seagrass ground truth data (Spectral Range 2). Bars show spectral ranges and red parts show pre-filtered data. Min denotes minimum and Max denotes maximum.

3.4.3 Supervised Classification

Six supervised classification frameworks were designed and applied to the multi-temporal Bahamas composite. These frameworks were based on the machine learning algorithm Random Forests by Breiman (2001) to solve the binary classification problem (Seagrass and Non-Seagrass). This classifier uses multiple self-learning decision trees to allocate pixels to given classes and is robust regarding outliers and noise (Breiman, 2001). Following the classification procedure of the ACA, the number of trees was set to 15 and the number of seeds to 42 (Lyons et al., 2020). The classifier was used in a probabilistic mode to allow for a soft classification. Therefore, it generated a per-pixel probability of 0 to 100% determining how likely it is that a given pixel is seagrass. The probability threshold over which a pixel is assigned to the Seagrass class was chosen after examination of the accuracy assessments (Chapter 4.3.4). Five thousand points per class were used to train the classifier, and 500 additional and independent points per class to validate it. These points were extracted from the image via stratified sampling of the first five Sentinel-2 bands.

The six classification frameworks (Figure 3) can be divided into three main models which were run twice, each using two different spectral ranges (Spectral Range 1 and Spectral Range 2 of Chapter 3.4.2). The first model (ClassBased) used the harmonised ACA classified data as training data (TD), and the ground truth data as validation data (VD). To not cause spatial auto-correlation between TD and VD, a 2,000 m buffer was created around the VD and used to mask underlying pixels before TD points were sampled. The second model (GeoSplit 1) used only ground truth data which was split into TD and VD depending on location. Ground truth data in the north of the image was assigned TD, and ground truth data in the south was assigned VD. The third model (GeoSplit 2) followed a similar approach to GeoSplit 1, but used the northern part of the ground truth data as VD, and the southern part as TD. These GeoSplit-models were created to further minimise geospatial auto-correlation.

Classification Model	**Spectral Range**	**Training Data**	**Validation Data**
ClassBased	1	ACA Classified data	Ground truth data
	2	ACA Classified data	Ground truth data
GeoSplit 1	1	Northern ground truth data	Southern ground truth data
	2	Northern ground truth data	Southern ground truth data
GeoSplit 2	1	Southern ground truth data	Northern ground truth data
	2	Southern ground truth data	Northern ground truth data

Table 3: Overview of used classification frameworks. Spectral Range 1 and 2 refer to Chapter 3.4.2. ACA denotes Allen Coral Atlas.

3.4.4 Accuracy Assessment

The overall accuracy (OA), producer's accuracy (PA), user's accuracy (UA), and the F1-score (harmonised mean of PA and UA) of both classes were estimated for each probability threshold between 0 and 100% in increments of 1. These metrics were based on the following equations (Story and Congalton, 1986):

$$OA = \frac{Number\ of\ correctly\ classified\ pixels}{Number\ of\ VD\ pixels} \tag{9}$$

$$PA = \frac{Number\ of\ correctly\ classified\ pixels\ in\ each\ class}{Number\ of\ VD\ pixels\ of\ the\ same\ class} \tag{10}$$

$$UA = \frac{Number\ of\ correctly\ classified\ pixels\ in\ each\ class}{Total\ number\ of\ VD\ pixels\ classified\ as\ the\ same\ class} \tag{11}$$

$$F1 - score = 2 * \frac{UA * PA}{UA + PA} \tag{12}$$

3.4.5 Seagrass Area Estimation

The results of the accuracy assessment were then used for a quantitative comparison of the classification frameworks. Furthermore, the probability threshold for which the F1-score of the Seagrass class drops nearest to 100% probability determined the threshold over which a pixel is assigned Seagrass. The two classification frameworks which yield the highest F1-score at the determined probability threshold were used to set the minimum and maximum habitat extent. To assess the protected area of seagrass, the UNEP-WCMC (2021) MPAs were used. Moreover, the seagrass habitat extent was compared to the total EEZ area, the mapped shallow water area, and the ACA seagrass extent.

3.5 Carbon Stock and Sequestration Potential Calculation

Country-scale carbon stock ranges were calculated following the Tier 1 and Tier 2 approach of The Blue Carbon Initiative (2014). These approaches represent different levels of certainty. Tier 1 assessments are based on published IPCC (Intergovernmental Panel on Climate Change) default values of globally averaged carbon estimates and show a lower level of certainty. A higher accuracy and certainty is reached through Tier 2 assessments, which use country-specific in-situ data (The Blue Carbon Initiative, 2014). For the latter assessment, values estimated in Chapter 3.2.1 were used. Minimum carbon range values were multiplied with the minimum classified seagrass extent, and maximum carbon range values were multiplied with the maximum seagrass extent.

Country-scale sequestration potentials were calculated using the minimum and maximum seagrass extent and the country-specific average sequestration rates collected in Chapter 3.2.1. To compare each country's sequestration potential with their emissions, carbon was converted to CO_2 following Fourqurean et al. (2012):

$$CO_2 = 3.67 * Carbon \tag{13}$$

4 Results

Due to the lack of TD and VD for seagrass classification, only one out of ten countries was classified. The following results for carbon and emission data acquisition, image pre-processing, habitat classification, and seagrass area and carbon calculations therefore apply only to The Bahamas.

4.1 Auxiliary Data Acquisition

This chapter summarises the findings for country-specific carbon stock inventories and emissions.

4.1.1 Seagrass Carbon Data

Globally averaged estimates for carbon stocks of the seagrass ecosystem (Tier 1 assessment) range from 910 to 82,900 Mg carbon per km^2 (Table 4), with an average of 10,800 Mg carbon per km^2 (IPCC, 2014).

The systematic technical review for Bahamian carbon stocks (Tier 2 assessment) shows a range between 15,417.55 Mg carbon per km^2 and 16,486.47 Mg carbon per km^2, with an average of 15,952.01 Mg carbon per km^2 (Buchan, 2000; Dierssen et al., 2010; Fourqurean et al., 2012; van Tussenbroek et al., 2014). Total biomass carbon accounts for 2.12% (327.55 Mg C km^{-2}) of the minimum carbon, and for 6.48% (1,068.92 Mg C km^{-2}) of the maximum one. These numbers are based on the three occurring species *Thalassia testudium*, *Syringodium filiforme*, and *Halodule wrightii*. Soil carbon therefore accounts for more than 90% of the total carbon stock range, and is based on averaged bio-regional data due to the lack of Bahamian soil carbon inventories.

Tier 2 ranges fall within the global averaged estimates, with a minimum 14,507.55 Mg carbon per km^2 greater than the Tier 1 minimum, and a maximum 6,413.53 Mg carbon per km^2 lower than the Tier 1 maximum.

Sequestration rates for Bahamian seagrass average 0.0026 Mt CO_2 per km^2 per year (Alongi, 2018; Dierssen et al., 2010).

	Carbon Stock Minimum [Mg/km^2]	Carbon Stock Maximum [Mg/km^2]	Source
Tier 1	910.00	82,900.00	IPCC (2013)
Tier 2	15,417.55	16,486.47	Buchan (2000); Dierssen et al. (2010); Fourqurean et al. (2012); van Tussenbroaek et al. (2014)

Table 4: Seagrass carbon stock ranges for Tier 1 (global average) and Tier 2 (country-scale) assessments based on IPCC (2014); Buchan (2000); Dierssen et al. (2010); Fourqurean et al. (2012); van Tussenbroek et al. (2014).

4.1.2 Carbon Emissions

In 2018, Bahamian CO_2 emissions from the use of coal, gas, and oil equaled 1.81 Mt and accounted for 0.0049% of the world's emissions. Between the years of 1985 and 2018 CO_2 emissions averaged 1.87 Mt, with a trough of 2.86 Mt in 1986 and a peak of 1.41 Mt in 2013 (Figure 11) (Friedlingstein et al., 2020).

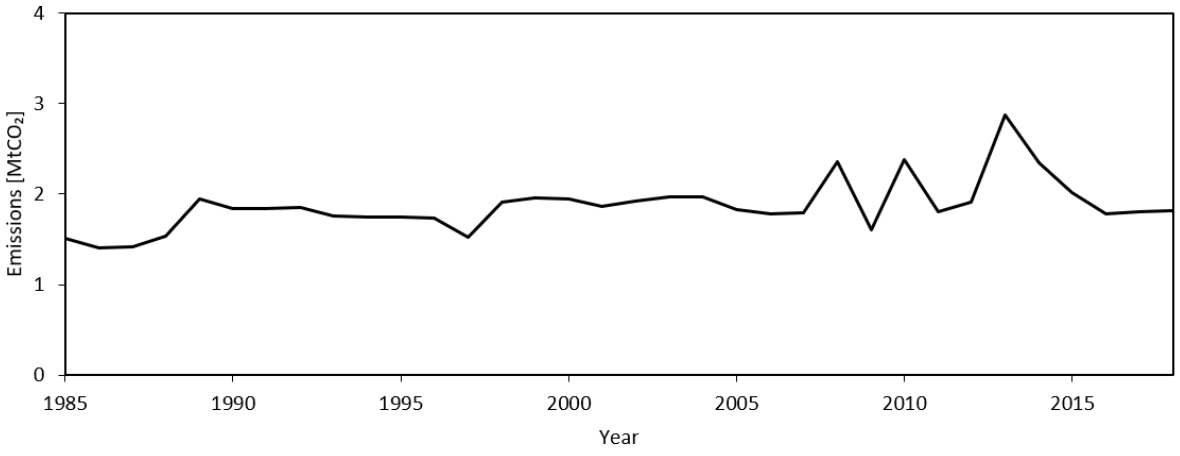

Figure 11: Carbon emissions of The Bahamas between 1985 and 2018 (Friedlingstein et al., 2020).

4.2 Image Pre-Processing

The image pre-processing results include the achieved environmental noise values, masking thresholds and the pre-processed composite.

4.2.1 Environmental Noise

The environmental noises for the tile-centered deep water polygon (Polygon 1) of The Bahamas range from 0.000151 to 0.000211 sr^{-1}, therefore falling within the limits of optimal noise (<0.00025 sr^{-1}) (Dörnhöfer et al., 2016; Giardino et al., 2015) (Table 5). This limit is not met by the noise of the polygon placed on overlapping tile edges (Polygon 2), which achieved values between 0.00035 and 0.000608 sr^{-1}. Both polygons show minimal environmental noises in B11, and maximum noises in B2.

Band	**Environmental Noise [sr^{-1}] Polygon 1**	**Environmental Noise [sr^{-1}] Polygon 2**
B2	0.000211	0.000608
B3	0.000191	0.000510
B4	0.000165	0.000460
B8	0.000162	0.000429
B11	0.000151	0.000336

Table 5: Environmental noise of the below-surface reflectance (R_{rs}) of optically deep water using two 32x32 pixel area polygons and standard deviations for the bands B2 (Blue), B3 (Green), B4 (Red), B8 (Near Infrared), and B11 (Shortwave Infrared 1).

4.2.2 Masking Efforts

All histograms used for the Otsu-based maskings achieved bi-model distributions (Figure 12). The land masking threshold based on the MNDWI equals 0.15, the optically deep water masking threshold based on the Shallow Water Index is -0.43, and the MNDWI threshold for optically deep water masking equals 0.27.

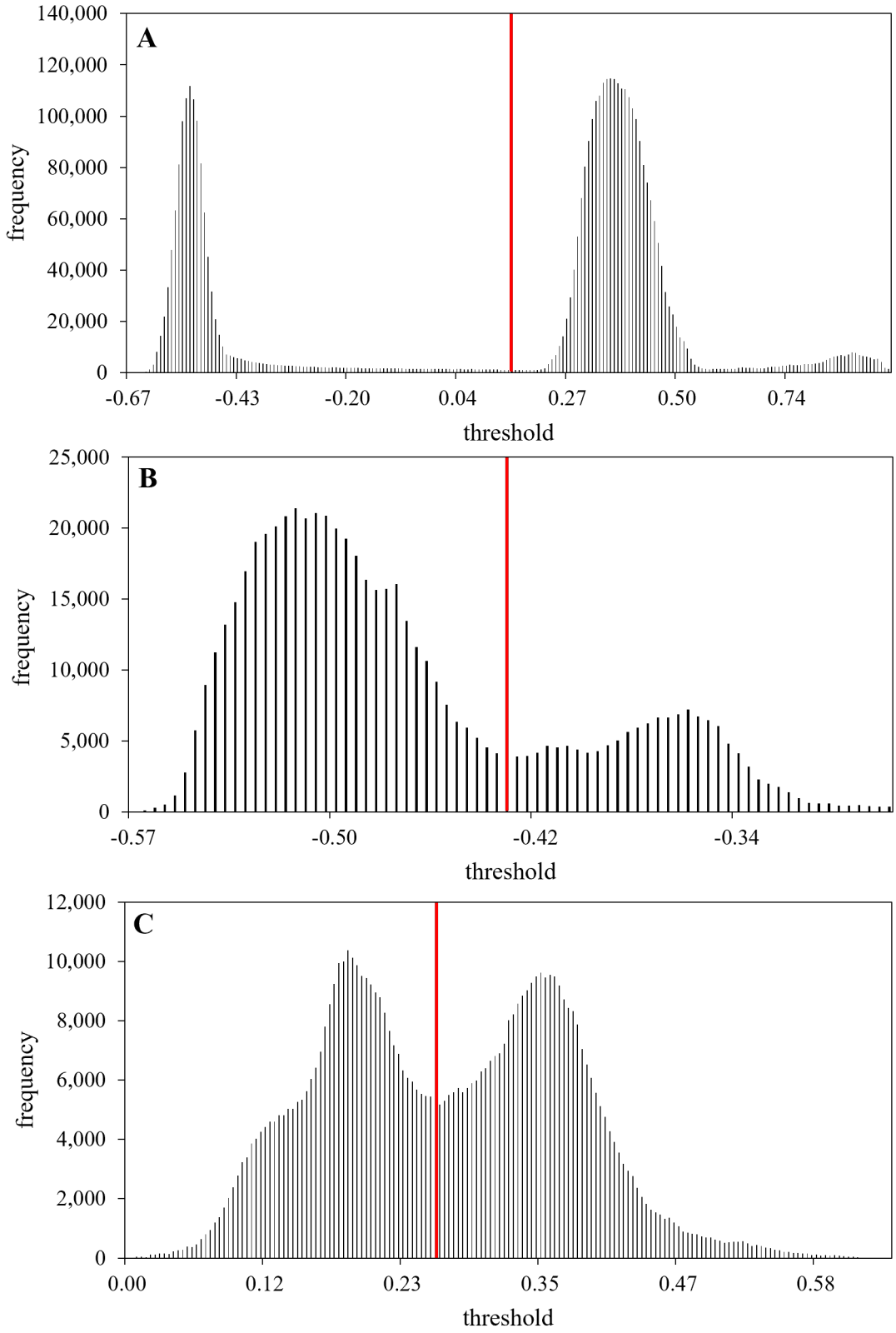

Figure 12: Histograms and thresholds (red) for A) MNDWI-based land masking, B) Shallow Water Index-based and C) MNDWI-based optically deep water masking.

4.2.3 Pre-Processed Image

Figure 13 displays the pre-processed Sentinel-2 2A r_{rs} image, as well as a nautical chart for the same region. Non-masked water areas match depth levels of less than 25 metres (Landfall, 2021). Optically shallow waters cover an area of 114,059.25 km^2, which equals 18.40% of the total Bahamian EEZ.

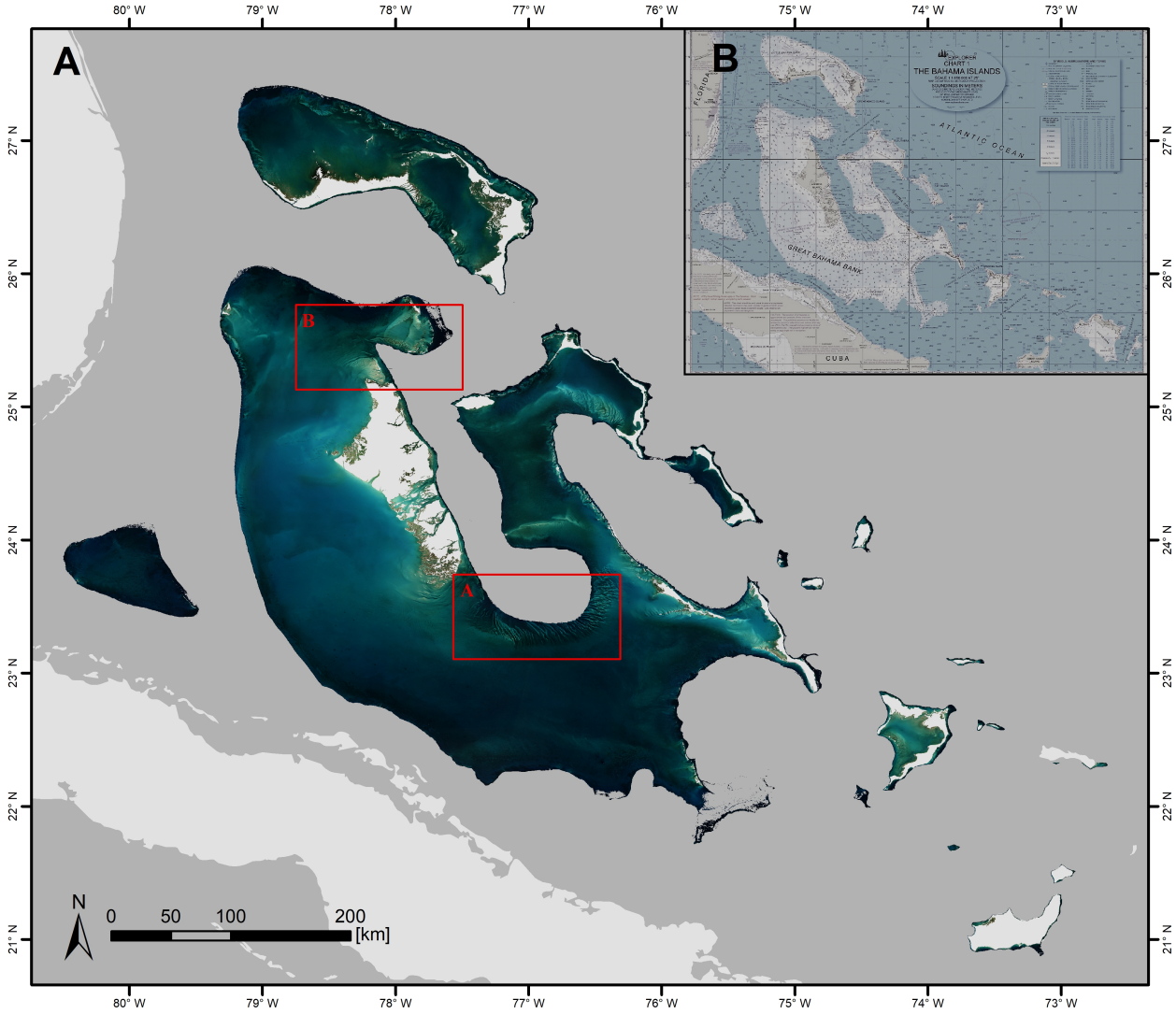

Figure 13: A) True colour below surface-reflectance Sentinel-2 composite of The Bahamas. B) Nautical chart of The Bahama Islands (Landfall, 2021). Red boxes represent the location of the insets of Figure 19.

4.3 Seagrass Classification

The following classification results cover both the unsupervised and supervised classification, as well as the data preparation and accuracy assessment.

4.3.1 Unsupervised Classification

The unsupervised classification (Figure 14) illustrates an overlap of Seagrass ground truth data with pixel clusters one, two, and three. Non-Seagrass overlaps each of the five identified clusters. Due to this, no clear allocation of the existing habitat classes to produced pixel clusters is possible, necessitating a supervised classification.

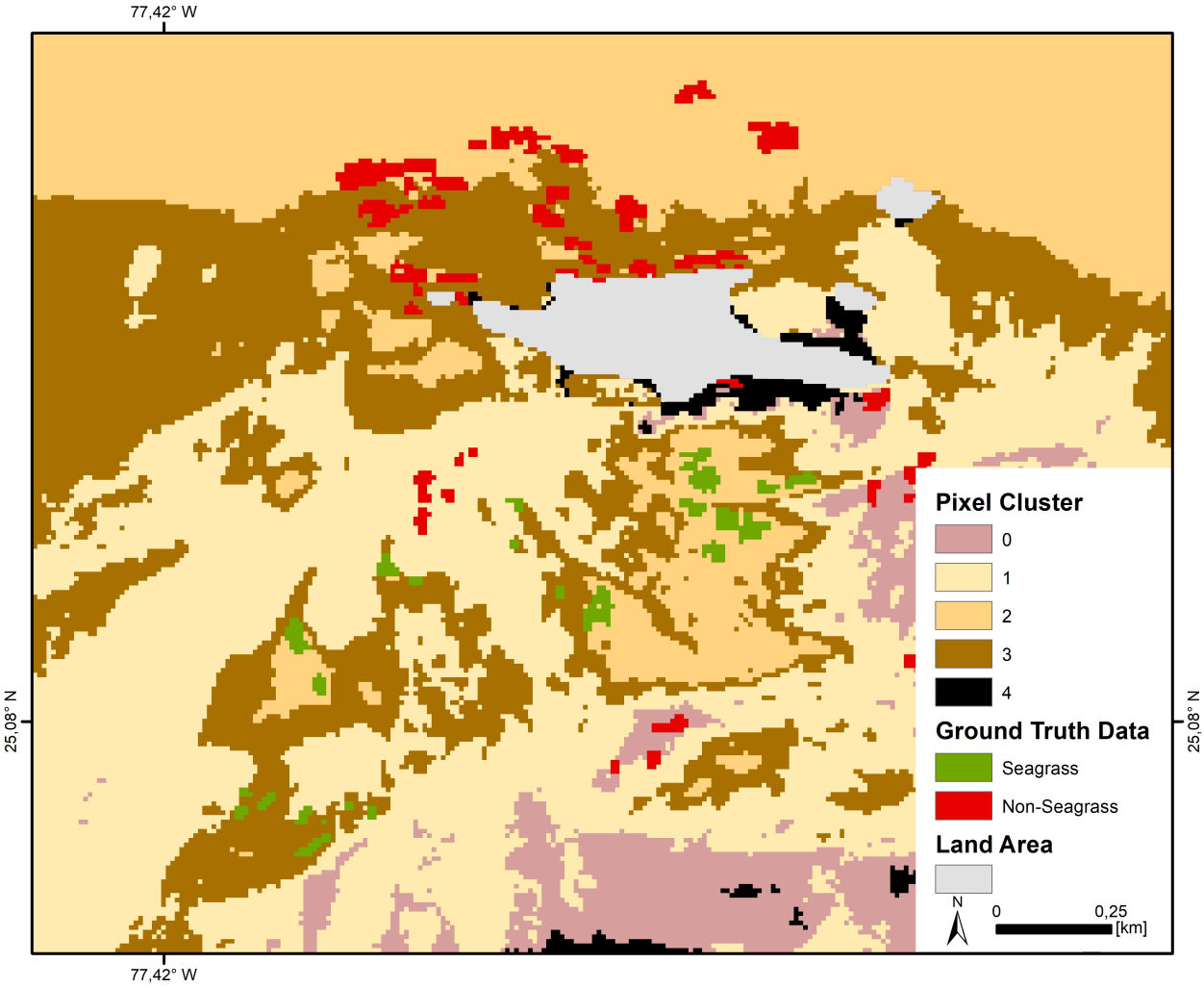

Figure 14: Unsupervised marine habitat classification for The Bahamas using five clusters, overlaid with Seagrass and Non-Seagrass ground truth data of the Allen Coral Atlas (Allen Coral Atlas, 2020).

4.3.2 Input-Data Preparation

Figure 15 displays the boxplots of r_{rs} spectral ranges for the ground truth and ACA classified data before (Original Range) and after (Spectral Range 1 and 2) the harmonisation procedure was applied (Chapter 3.4.2). Throughout all plots and bands, the Seagrass class shows lower spectral ranges than the Non-Seagrass class. The averaged median for all Seagrass bands is 0.02 sr^{-1} and 0.04 sr^{-1} for Non-Seagrass. Moreover, the ranges for Seagrass bands cover less spectral values than the Non-Seagrass ranges.

The ACA classified data shows greater original spectral ranges than the ground truth data, especially for Band 5. Spectral Range 1 covers the same minimums and maximums for both data sets, while the ranges for classified data are reduced compared to the original. Spectral Range 2 shows the same ranges for the Non-Seagrass class, but reduced ranges for the Seagrass class.

Bands B1 to B4 of the ground truth data represent non-overlapping interquartile ranges of the Seagrass and Non-Seagrass classes and show the strongest difference within Spectral Range 2. Within the ACA classified data, all bands show at least partly overlapping interquartile ranges, while those of Seagrass lie fully within the ranges of Non-Seagrass pixels for B2 and B3 of the Original and Spectral Range 1. For Spectral Range 2, the interquartile ranges do not entirely overlap and the 25^{th} percentile of Seagrass and the 75^{th} of Non-Seagrass show values of a smaller difference than those of the other spectral ranges.

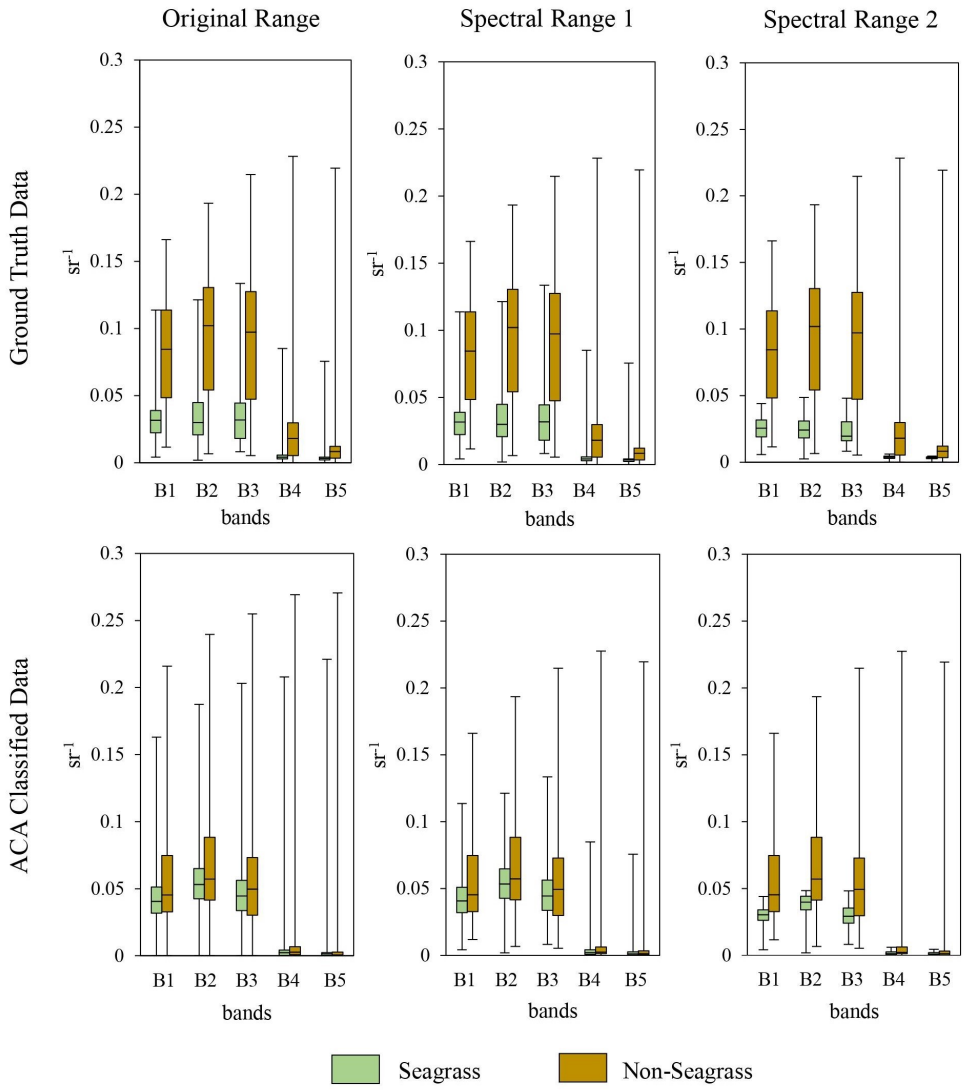

Figure 15: Spectral ranges of the ground truth and ACA classified data for the first five Sentinel-2 below-surface reflectance (r_{rs}) bands, divided into Seagrass and Non-Seagrass classes. Original Range shows non-processed ranges, Spectral Range 1 shows the ACA classified data harmonised with the minimum and maximum of the ground truth data, Spectral Range 2 shows the same Non-Seagrass ranges as Spectral Range 1 and the Seagrass ranges harmonised with the 80th percentile of the Seagrass ground truth data. ACA denotes Allen Coral Atlas.

4.3.3 Training and Validation Data

The TD of the supervised classification model ClassBased shows a stronger overlap of the interquartile ranges of Seagrass and Non-Seagrass within Spectral Range 1 than within Spectral Range 2 (Figure 16). VD shows non-overlapping interquartile ranges for both spectral range ver-

sions, and represent the strongest difference within Spectral Range 2.

GeoSplit 1, which is based on ground truth data, also shows non-overlapping interquartile ranges for VD of both ranges, with stronger differences within Spectral Range 2. TD of Spectral Range 1 shows overlapping interquartile ranges, but Spectral Range 2 does not.

GeoSplit 2 shows GeoSplit 1's inverted TD and VD boxplots for both spectral ranges.

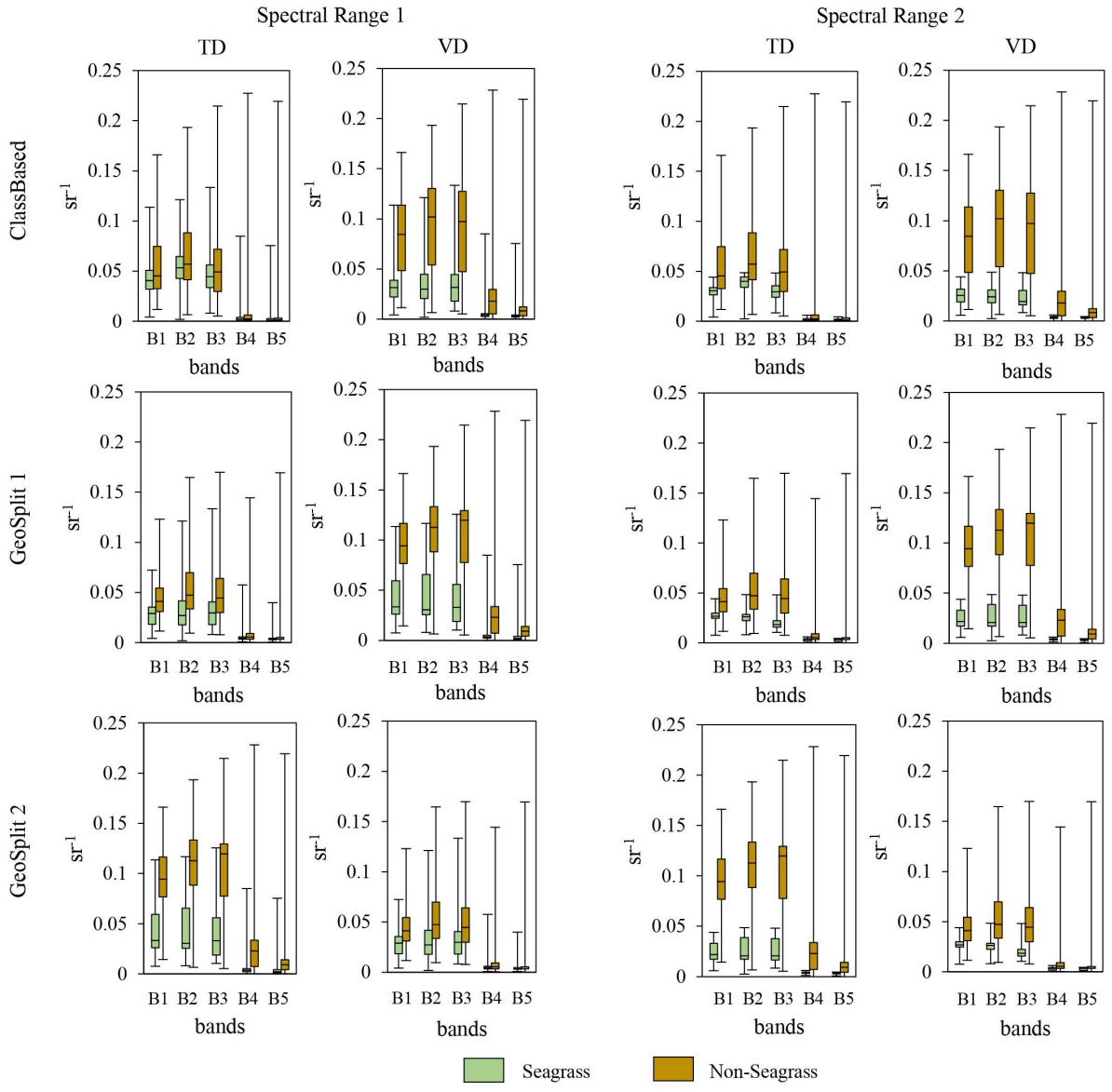

Figure 16: Spectral ranges of the training (TD) and validation data (VD) for the first five Sentinel-2 below-surface reflectance (r_{rs}) bands, divided into Seagrass and Non-Seagrass classes for the six supervised classification frameworks described in Chapter 3.4.3.

4.3.4 Accuracy Assessment

Figure 17 shows the OAs and F1-scores of Seagrass and Non-Seagrass for the six supervised classification frameworks. OAs of all frameworks, except GeoSplit 2 Spectral Range 1, drop towards higher seagrass probabilities until a 50% score is reached. The averaged OA has its minimum at 60.53% for GeoSplit 2 Spectral Range 1, and its maximum at 77.79% for ClassBased Spectral Range 2. Moreover, each model yields a higher maximum and averaged OA using Spectral Range 2.

F1-scores for Seagrass follow a similar pattern to OAs, but drop until a score of 0% is reached. Scores for Spectral Range 1 show more abrupt drops at lower probabilities (between 5 and 25%) than Spectral Range 2 (between 25 and 60%). F1-scores for Non-Seagrass show an inverted pattern to the ones of Seagrass, with scores starting at 0% and rising towards higher probabilities.

For both spectral ranges, F1-scores intersect at probability thresholds lower than 50%. Both F1-scores of Spectral Range 2 show similar values with lower probabilities, while scores of Spectral Range 1 do not follow this pattern.

The probability threshold for which the F1-score of the Seagrass class drops nearest to 100% probability is 60% and therefore determines the threshold over which a pixel is assigned Seagrass. At this threshold, the two highest F1-scores are 75.38% (GeoSplit 2 Spectral Range 2) and 64.99% (ClassBased Spectral Range 2). Therefore, these two classification frameworks define the minimum and maximum seagrass area extent. These frameworks reach OAs of 77.60% and 72.20%, PAs of 68.60% and 51.60%, and UAs of 83.65% and 87.75%, respectively. F1-scores for Non-Seagrass are at 86.60% and 76.95%, PAs at 86.60% and 92.80%, and UAs at 73.39% and 65.72%, respectively. For both classification models, Seagrass achieves lower PAs, but higher UAs than Non-Seagrass.

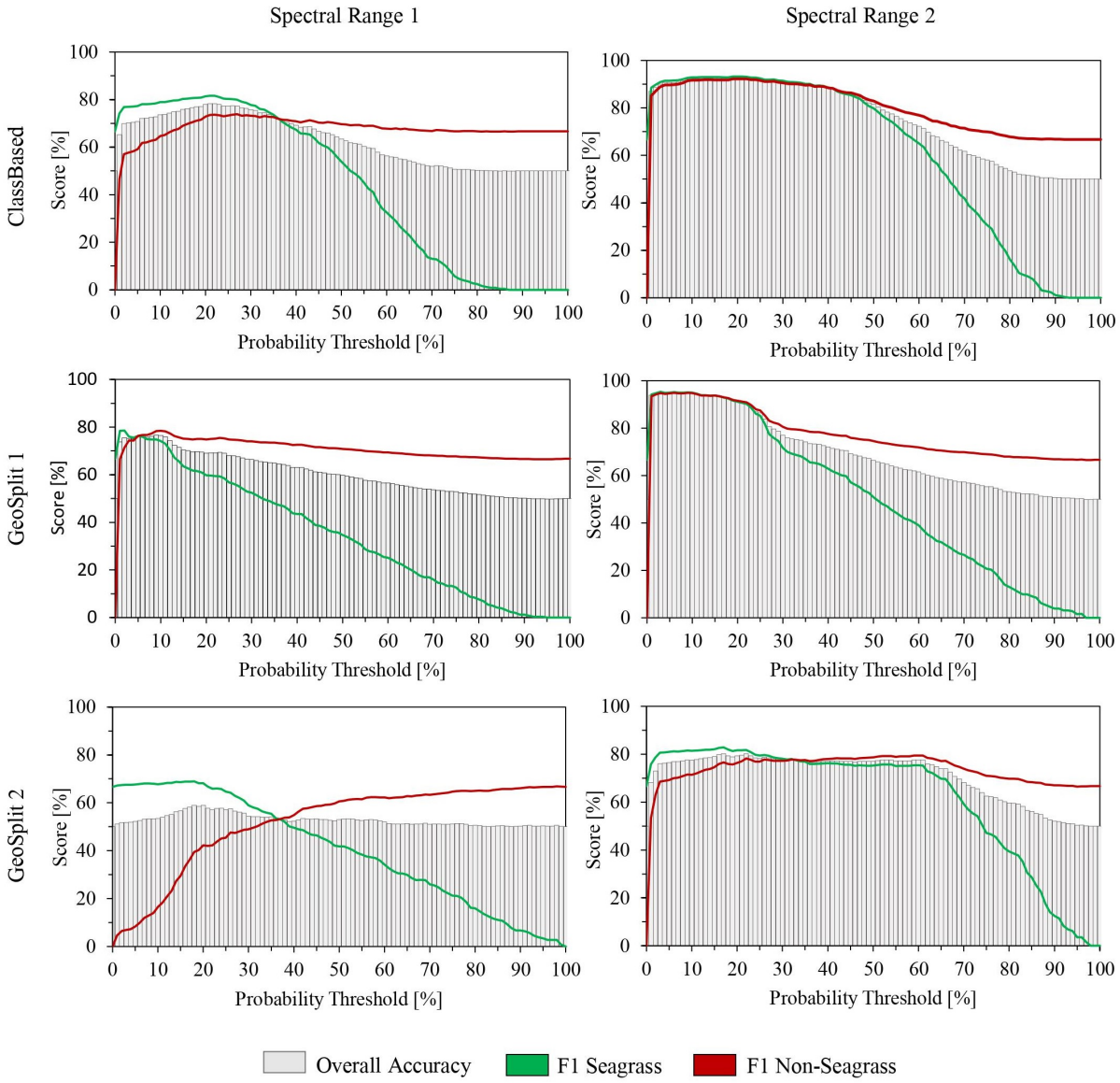

Figure 17: Overall Accuracy, F1-score for Seagrass, and F1-score for Non-Seagrass for the six applied classification frameworks.

4.3.5 Seagrass Area Estimation

Based on the 60% probability threshold of the soft classification, the minimum seagrass extent for The Bahamas is 11,779.44 km^2 and the maximum 27,629.32 km^2 (Figure 18). The minimum extent is based on the classification framework GeoSplit 2 Spectral Range 2, and the maximum is based on ClassBased Spectral Range 2. Bahamian seagrass covers between 1.90 and 4.46% of the country's EEZ, and 10.33 and 24.22% of its shallow area. About 6 to 11% of its extent lies within MPAs. The mapped seagrass extent equals 25.29 to 59.31% of the area mapped by the ACA.

GeoSplit 2 Spectral Range 2 (Figure 18 1A) shows large areas of low and medium probability (white to medium green; 0 to 66% probability), and a comparatively small area of high probability (dark green; >66% probability), while ClassBased Spectral Range 2 (Figure 18 2A) shows large areas of low and high probability (white and dark green respectively), and small areas of medium probability (medium green). The classified maximum extent of seagrass (Figure 18 2B) identifies vaster meadows in the south and east of The Bahamas than the minimum extent (Figure 18 1B). Figure 19 illustrates a detailed comparison of the minimum and maximum mapped seagrass extent, and the ACA classification results.

Boxplots for the classified seagrass extents of all six classification frameworks are illustrated in Figure 20. The interquartile ranges of ClassBased Spectral Range 2 show less overlap than within Spectral Range 1, in which those of Seagrass fall entirely within those of Non-Seagrass. For GeoSplit 1 the least overlap is identified within Spectral Range 1, while the interquartile ranges of Seagrass of Spectral Range 2 fall within those of Non-Seagrass. GeoSplit 2 shows only small interquartile range overlaps with Spectral Range 1, and small or no overlaps within Spectral Range 2.

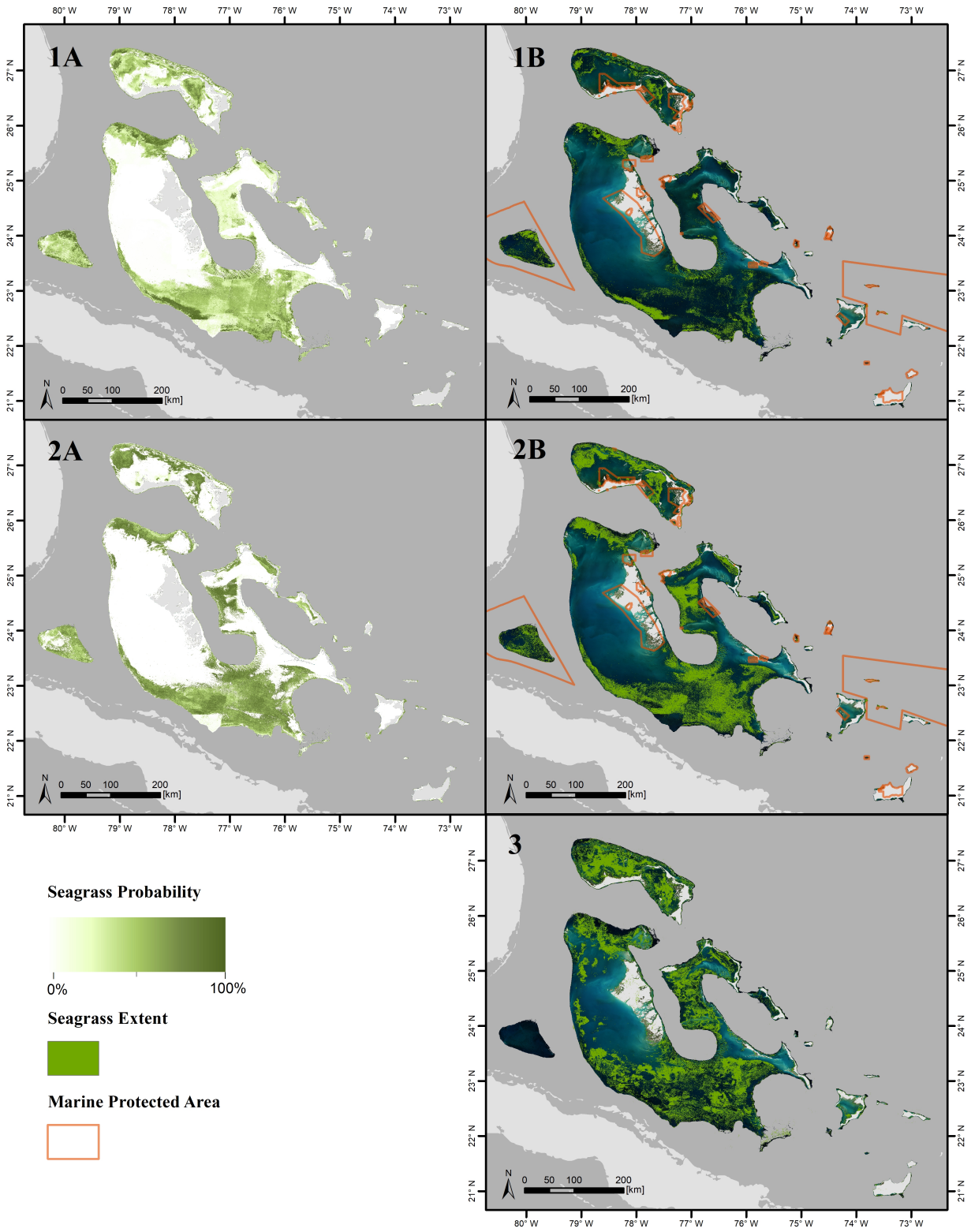

Figure 18: Soft probability for seagrass using the classification model GeoSplit 2 Spectral Range 2 (1A) and ClassBased Spectral Range 2 (2A); Below surface-reflectance Sentinel-2 (r_{rs} S2) composite overlaid with the minimum (1B) and maximum (2B) classified seagrass extent based on 60% soft probability threshold of 1A/2A) and Marine Protected Areas (UNEP-WCMC, 2021); r_{rs} S2 composite overlaid with the seagrass extent by the ACA (3) (Allen Coral Atlas, 2020).

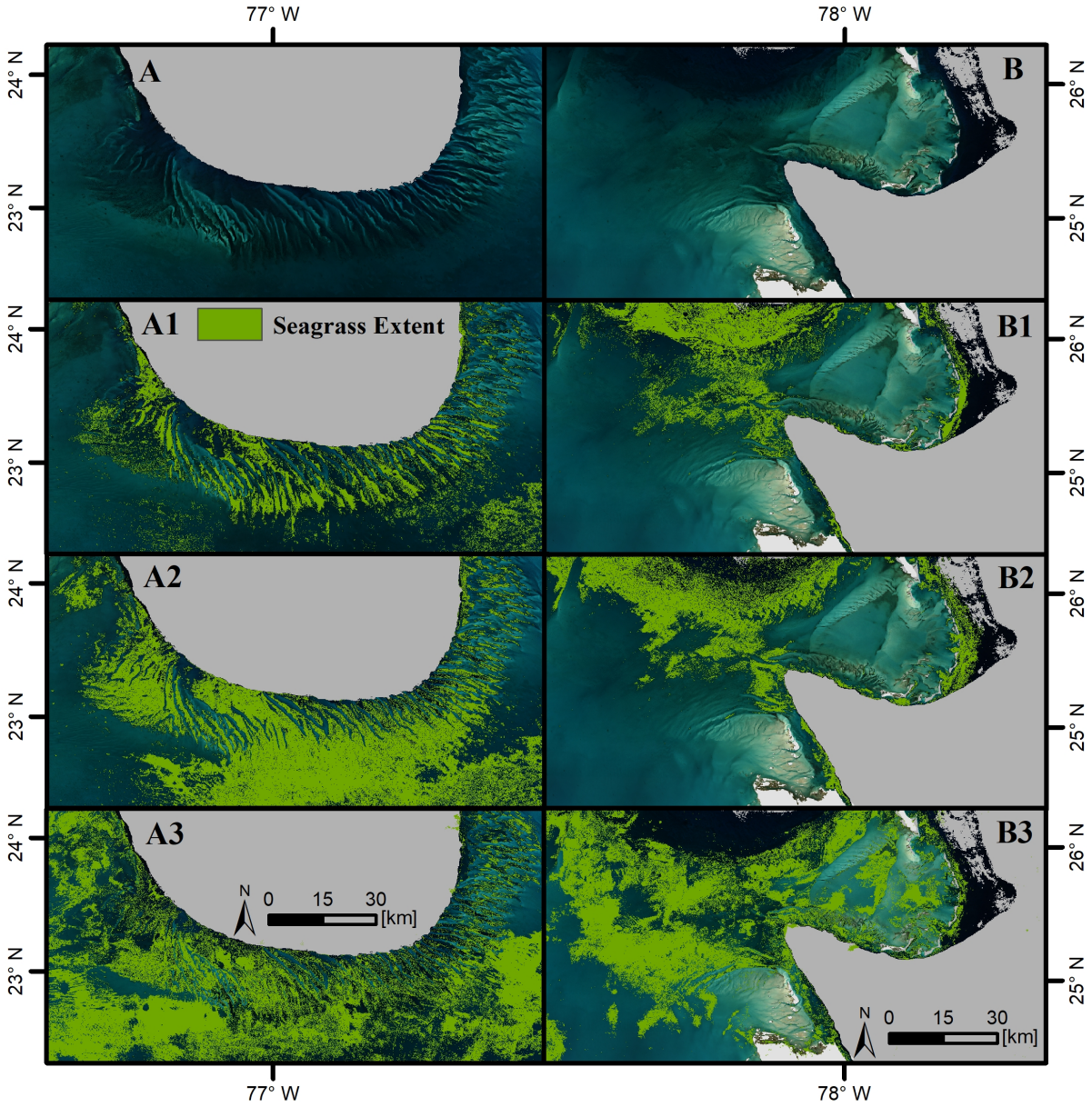

Figure 19: True colour below surface-reflectance Sentinel-2 composite of The Bahamas overlaid with the minimum (A1, B1), maximum (A2, B2), and ACA (A3, B3) seagrass extent (Allen Coral Atlas, 2020). Location of A and B is represented in Figure 13.

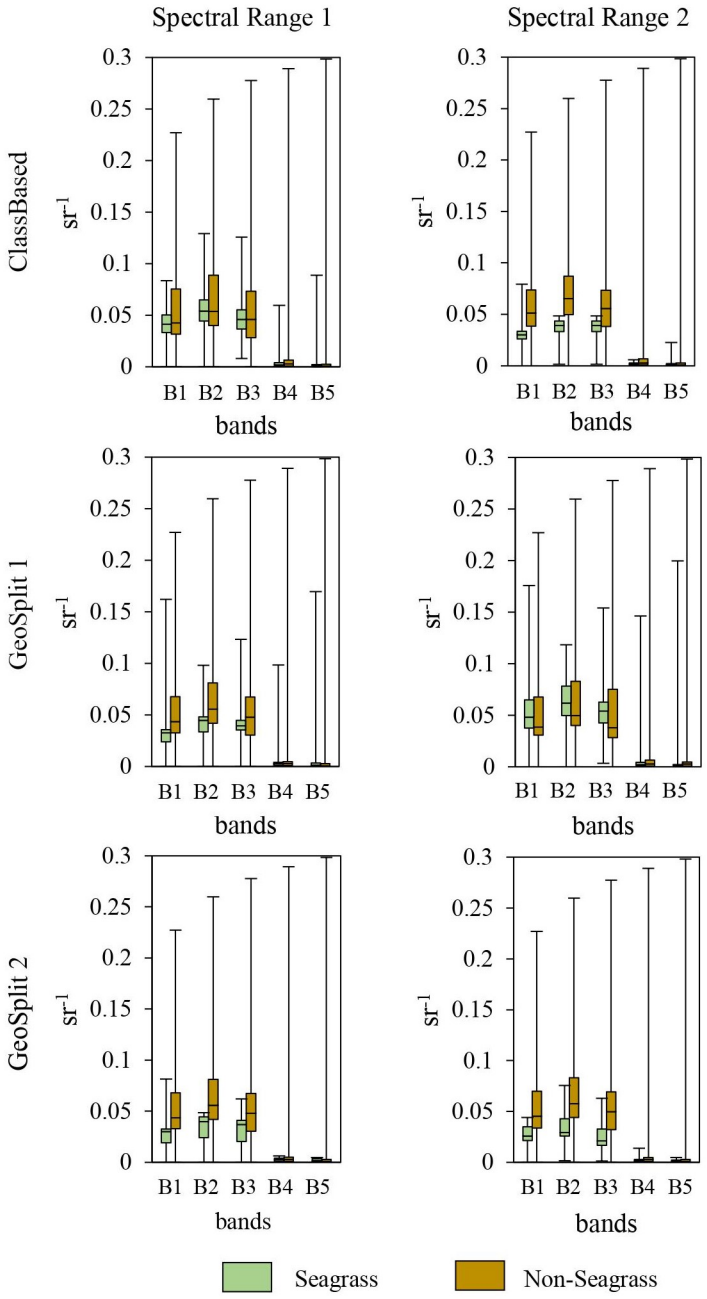

Figure 20: Spectral ranges of classified seagrass and non-seagrass area for the first five Sentinel-2 below-surface reflectance (r_{rs}) bands of the six applied classification frameworks.

4.4 Carbon Stocks and Sequestration Potential

Based on the globally averaged estimates of the Tier 1 assessment, Bahamian seagrass stores between 10,719,288.91 and 2,290,470,292.26 Mg carbon (Table 6). The country-specific Tier 2 assessment shows carbon stock values between 181,610,083.57 and 455,509,862.63 Mg. Tier 2 ranges fall within the global averaged estimates, with a minimum of 170,890,794.66 Mg greater, and a maximum of 1,834,960,429.63 Mg lower than the Tier 1 ranges.

	Carbon Stock Minimum [Mg]	**Carbon Stock Maximum [Mg]**
Tier 1	10,719,288.91	2,290,470,292.26
Tier 2	181,610,083.57	455,509,862.63

Table 6: Tier 1 and 2 carbon stock minimums and maximums in Megagram for Bahamian seagrass.

Bahamian seagrass yields the potential to sequester between 31.02 and 72.75 Mt CO_2 per year, which equals about 17 to 40 times the amount of carbon which was emitted by The Bahamas in 2018 (Friedlingstein et al., 2020).

5 Discussion

The following chapter will critically discuss the applied methods (Chapter 3) and results (Chapter 4) in order to evaluate if the set objectives (Chapter 1.2) were met. It will also put forward ideas for improvement.

5.1 Image Pre-Processing

This chapter examines the achieved environmental noise values and the pre-processed Sentinel-2 composite.

5.1.1 Environmental Noise

The environmental noise of optically deep water can be used to assess the effectiveness of image pre-processing steps like the cloud and sunglint removal (Chapter 3.3.2) (Sagar et al., 2014). Moreover, it functions as an indicator for the degree of accuracy and precision that can be achieved with marine habitat classifications (Brando and Dekker, 2003). Table 5 shows that the environmental noise of Polygon 1 falls within acceptable limits, indicating an effective pre-processing procedure and making tile-centered areas appropriate for further analysis and classifications. The noise levels of Polygon 2, on the other hand, exceed the acceptable limits, indicating problems within the pre-processing at tile edges, which can influence habitat mapping.

An optical assessment of the multi-temporal composite supports the assumption of an overall effective environmental noise filtering since no clouds or sunglint effects are apparent and habitats are clearly visible. This is also due to the fact that a multi-temporal approach minimised the effects of visible waves. However, some areas (Figure 21) show artifacts of cloud shadows, which could cause misclassification of seagrass due to their dark colours. The effects of unsatisfactory noise levels at tile edges can be identified in the southern part of the Great Bahama Banks (Figure 22), where lines of overlapping tiles are visible. These lines also have an effect on the classification results which will be discussed in Chapter 5.2.3.

Cloud shadow artifacts are likely caused by the utilisation of the 20^{th} percentile composition approach (Chapter 3.4.2) since it allocates the darkest pixels to the composite. The observed north to south running striping patterns are likely caused by Sentinel-2's staggered positioning of detectors, leading to different viewing angles for odd and even view detectors. This parallax effect

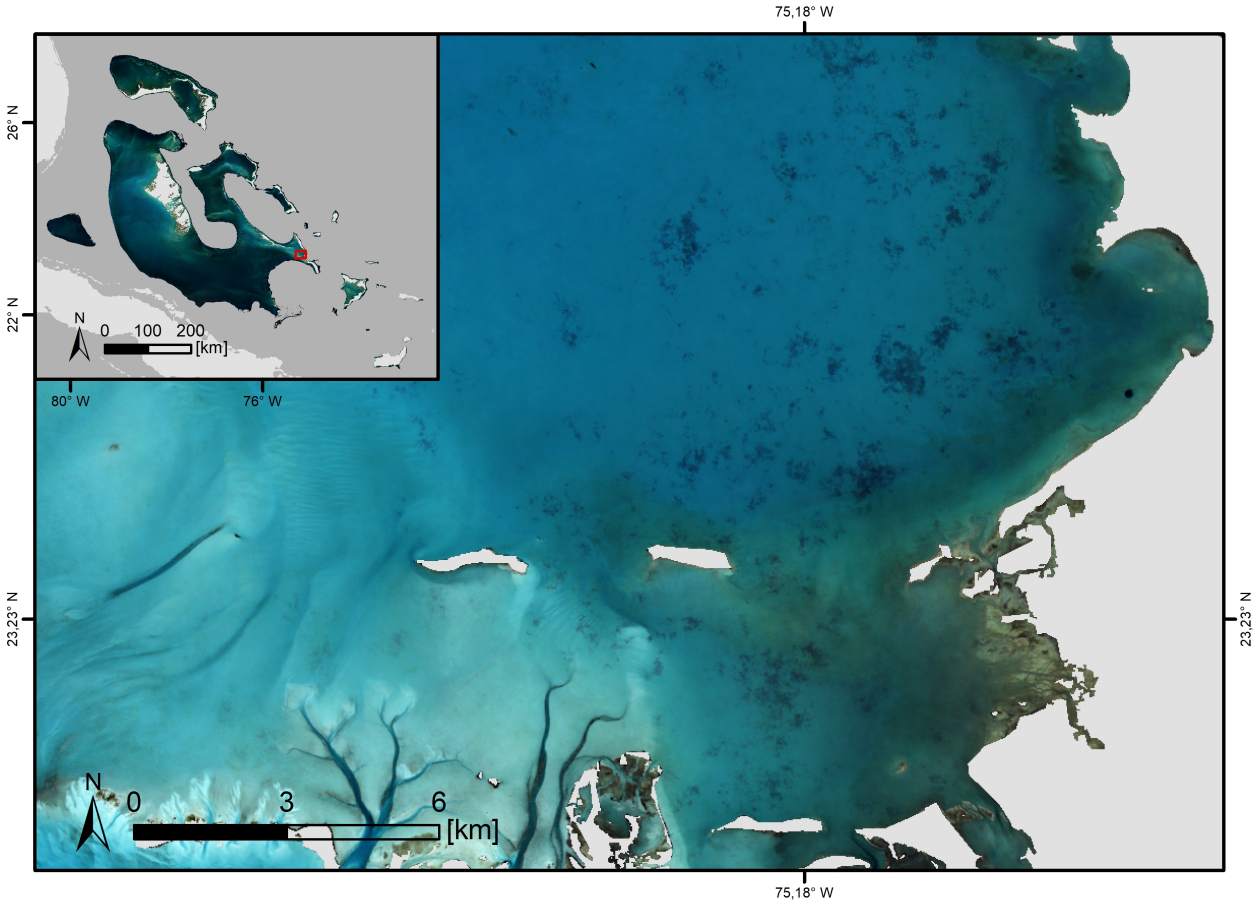

Figure 21: Sentinel-2 true colour composite of The Bahamas shallow water area with cloud shadow artifacts (dark patches).

is strongest over sunglint polluted areas and increased at scene borders (ESA, 2021). Therefore, enhanced sunglint removal is necessary to create seamless high-quality mosaics. This could be achieved through metadata-based filtering of single images, which combines sensor viewing and sun angles to minimise the possibility of sunglint (Kay et al., 2009). Another proxy for sunglint can be the high reflectance in near-infrared wavelengths over optically deep water, which can be used in regression models to adjust pixel values of shorter wavelengths (Hedley et al., 2016). Moreover, areas of stacked overlapping tile edges are created using more pixels than the surrounding areas, possibly causing the visible difference between tiles. This can be the reason for additional horizontally running lines within the composite. Enhanced sunglint filtering yields the potential to minimise this problem by decreasing the amount of pixels used for the composite. Using the geometric features of tiles to exclude overlapping areas could further improve the composite.

Environmental noise performs as a good first quantitative indicator for the quality of the pre-processed Bahamas composite, but lacks significance considering the large extent of the study

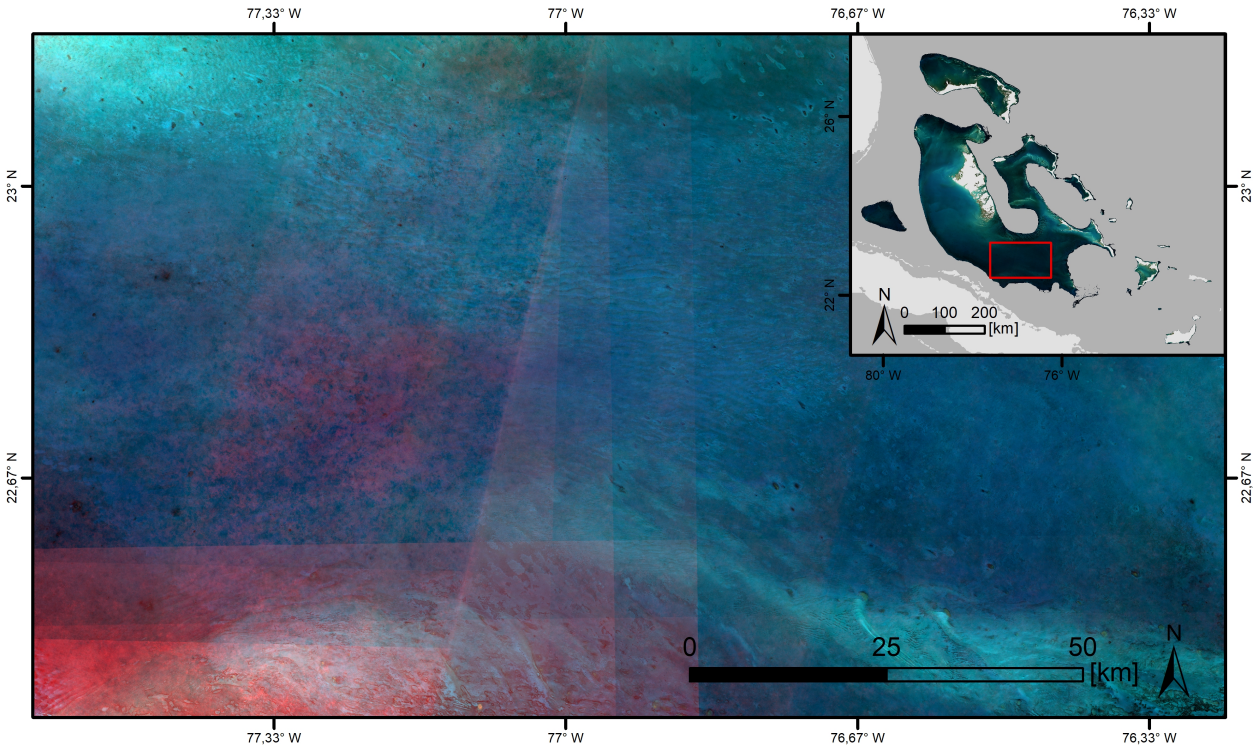

Figure 22: Sentinel-2 true colour composite of The Bahamas shallow water area with stretched red-band values for stronger tile edge visualisation.

area. There is a possibility for strong spatial variability of noise caused by The Bahamas spanning over multiple Sentinel-2 tiles. This is supported by the appearance of striping in only one part of the image. The implementation of multiple environmental noise polygons could help with a more solid assessment of the quality, but would still not cover each tile since some do not cover deep water areas. Furthermore, the environmental noise does not provide information about artifacts like cloud shadows.

5.1.2 Masking Efforts

Based on a visual assessment of the land and deep water masked image (Figure 13 A), and supported by a nautical chart (Figure 13 B), most areas which could lead to missclassification were masked successfully. The complexity of the Bahamian coastline demonstrates a challenging environment for the applied land masking method, since its very shallow water areas, sand- and mud-banks do not represent clear water-land edges (Figure 23). The use of the 20^{th} percentile reducer (Chapter 3.3.3) amplifies this complication through the utilisation of darker pixels which are more likely to be taken from low-tide satellite images and which feature value close to the land masking threshold (Traganos et al., 2021). This does not only demonstrate a challenge for the

algorithm, but also for the algorithm user who validates the land mask. There is a strong need for site specific information on near shore substrates. For this, it would be a cost-benefit advantage to include local authorities, scientists or volunteers to provide regional knowledge. The complexity of the Bahamian coastline with its countless small land patches (Figure 23) supports the use of a pixel-based masking approach over the use of country shapefiles, which cannot provide the needed precision. These shapefiles are nonetheless necessary for land water masking, but require manual adjustment in order to not cover coastal areas.

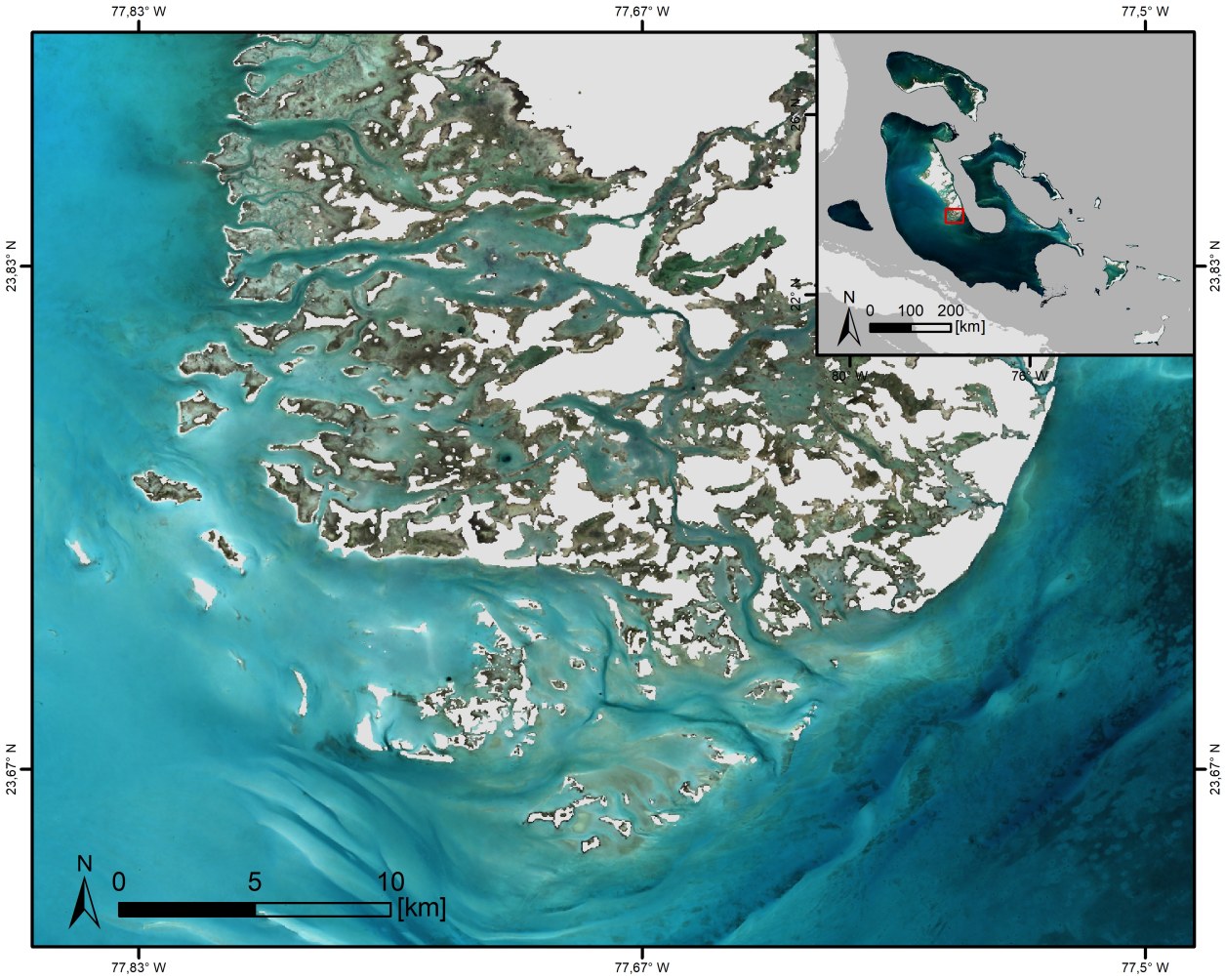

Figure 23: Sentinel-2 true colour composite of The Bahamas coastal area. Gray indicates land area.

The end result of the optically deep water masking is satisfactory and does not show unwanted deep water areas with which seagrass could be confused. A comparison of the nautical chart with the masked image shows the difference between deep water and optically deep water identified by the masking approach, since a small area of 2 to 22 m depths at 22°N, 76.5°W was masked. A visual assessment of the unmasked image shows this area in brighter colours than the surround-

ing water, suggesting that masking fails to identify this area as optically shallow. Analysing both applied indices separately reveals that the Shallow Water Index caused the masking of the aforementioned area, suggesting that the MNDWI is more suitable for identifying areas of more than 10 m depth, which are still visible to humans. Nevertheless, the combination of both indices is necessary in order to mask a sufficient deep water area and to minimise the manual masking efforts. The histograms of both applied optically deep water masks showed strong bi-modal distributions indicating a clear separability between optically deep and shallow waters (Figure 12). This high degree of separability was reached through the integration of user-defined bounding boxes which allowed for a specification of input pixels. The applied approach shows insufficient masking of deep waters close to the tile edges described in Chapter 5.1.1, making manual adjustments necessary. Therefore, an improved environmental noise filtering will also lead to an improved deep water masking. The introduction of additional indices could tackle further this problem. Feyisa et al. (2014) introduced the Automated Water Extraction Index for surface water mapping, which yields the potential to be adjustable for shallow water. Using a bathymetry dataset like ETOPO1 to mask depth-based deep water is useful but has to be handled with caution, since its 1 km spatial resolution is too coarse and shows inaccurate values in very shallow areas. Some near-shore areas which show depths of 1 to 2 m in the nautical chart are mapped with depth of up to 250 m. Therefore, it can only be used for waters of more than 1 km depth. The problem of unsatisfactory resolutions and accuracies within shallow waters is prevalent in most global bathymetry datasets, highlighting the need for country-specific bathymetry data (Thomas et al., 2021).

The assessment of the pre-processing procedure shows that an efficient algorithm was designed and that objective 1 of this thesis was achieved. However, there is still room for improvement.

5.2 Supervised Classification

The analysis of the supervised classification applies to the two classification models chosen for the minimum and maximum extent (Chapter 4.3.4).

5.2.1 Input-Data Preparation

In order to utilise class data from the ACA to map habitats using Sentinel-2, the finer resolution ACA data had to be matched with Sentinel-2's coarser resolution. This was achieved using a majority reducer on the ACA classified data, which was necessary since the ACA classified map still consisted of all five ACA classes. This reducer ensures that the created coarser pixel is assigned to the habitat which contributes most to its spectral profile. However, this approach leads to the creation of mixed pixels. Preventing this could be possible through the integration of a function which calculates the proportion of each class contributing to a pixel and discards it if none of the class proportions are above a set threshold. Figure 15 shows that the use of ground truth data's minimums and maximums to filter ACA classified data helps discard outliers, and therefore demonstrates a first harmonisation with true class values.

The seagrass ground truth data includes two classes: Dense and Sparse Seagrass. The latter class was discarded in order to not create mixed pixels caused by the coarser resolution of Sentinel-2. Similar to the ACA classified data, mixed pixels were also created when the resolution of the ground truth data was reduced. This mostly affects edges of seagrass meadows where one Sentinel-2 pixel covers both seagrass and the adjacent substrate. Ground truth data with brighter values was filtered out in order to reduce the number of mixed seagrass ground truth, and therefore also ACA classified, pixels. The boxplots of Spectral Range 2 (Figure 15) show the effectiveness of this method, reducing the overlap of interquartile-ranges between both classes and therefore creating a suitable data-input for training the classifier. However, this approach does not capture the complexity of the mixed pixel creation. Without a laborious analysis of the data, it is nearly impossible to estimate the amount of pixels affected by this, and how much they are affected. Therefore, it is difficult to estimate the correct percentile for filtering. An option to further decrease the number of mixed pixels could be the filtering of ground truth data before the resolution reduction. For this, single pixels and small clusters should be discarded since these lack the potential to cover enough spatial area to create a pure pixel. Moreover, Traganos and Reinartz (2018a) recommend the employment of a linear unmixing model for spatial resolutions higher than 5 m. These models

use defined classes and their spectra to decompose mixed pixels into class proportions (Keshava, 2003).

5.2.2 Classification Setup

Each model was assigned the same number of training and validation points per class to allow for a transparent comparison. The allocation of an equal amount of training points for both classes (5,000 for training and 500 for validation for a shallow water area of 114,059 km^2) also minimised the possibility of a biased classification, since machine learning algorithms often over-represent classes with larger training sample proportions (Millard and Richardson, 2015). Traganos et al. (2021) allocated a similar amount of Seagrass training data points (5,461) for a seascape area of similar size (128,741 km^2), but almost double the amount for Non-Seagrass (9,651). This indicates a stronger underestimation pattern of seagrass compared to the one of The Bahamas, which is supported by the recorded UA and PA (Traganos et al., 2021).

Millard and Richardson (2015) state that classification quality can be increased through the use of larger training samples sizes. Therefore, and based on the fact that the ACA classified data covers a wider spatial range than the ground truth data, an increase in training points for the ClassBased model could achieve enhanced classification results. The reason for this is that an increased number of points would cover more of the classes spatial variability. This approach would not change the classification results of the other models since the ground truth data is limited to a few homogeneous clusters without strong spatial variability. Amani et al. (2019) notes that even though an increase of training points is correlated to better classification results, it can cause efficiency reduction within GEE, and the use of under one million points is recommended.

Previous studies have shown that different levels of spatial separability for TD and VD have achieved different accuracies. Juel et al. (2015) observed an OA of 91.80% using spatially correlated data, while the use of spatially separated observations within sites achieved 81.90%. The OA achieved with data spatially separated between different sites was only 54.20%. Even though OAs are higher when data is more correlated, a minimisation of spatial proximity between TD and VD through buffering and geographical splits creates more reliable accuracies due to the reduction of collinearity (Juel et al., 2015; Millard and Richardson, 2015; Traganos et al., 2021).

Due to its ability to handle both normally and non-normally distributed data, and its robustness to outliers and noise, the Random Forest classifier has been implemented successfully in multi-

ple seagrass mapping approaches (Millard and Richardson, 2015; Breiman, 2001; Lyons et al., 2020; Traganos et al., 2021; Traganos and Reinartz, 2018c). These characteristics qualify it as a suitable classifier for mapping Bahamian seagrass considering the existing noisy TD. Classifier variables were set following the ACA classification procedure to simulate similar conditions for the ClassBased models compared to the ACA classified data on which it is based. However, both procedures use a different number of classes which could make a different approach necessary. For the classification of two classes within a similar sized area, Traganos et al. (2021) used viewer trees (ten) and seeds (zero). Moreover, the number of variables per split was set to two, while the square root of the number of used classes was chosen for the Bahamas. It would be beneficial to test settings used by other authors and also iterate through a variety of variables. Even though GEE provides many different settings for the Random Forest classifier, it still lacks the flexibility provided by other software like R (Hird et al., 2017). Furthermore, Shelestov et al. (2017) states that GEE classifiers are currently outperformed by neural network based approaches in terms of classification accuracy, indicating that these GEE functions require further improvement. Millard and Richardson (2015) suggest running iterative classifications based on the same variables to assess the stability of classified categories.

The Random Forest classifier was trained on Sentinel-2's first five bands with central wavelengths between 443 and 705 nm (ESA, 2015). This selection accounts for the fact that shorter wavelengths can penetrate deeper into the water column. Even though red light is completely absorbed at depths of more than 3 m, it is still useful for very shallow water seagrass and increases the complexity of the classifier (Åhlén et al., 2003). In order to define a class as precise as possible, it would be useful to integrate further feature bands. Additional bands could be generated by calculating the HSV parameters hue (H), saturation (S) and value (V) of the red-green-blue-image. Hue describes the pixel's colour, while saturation and value represent its illumination content (Hassanein et al., 2018). Another input feature could be the bottom-reflectance derived from r_{rs}, which has already been used to classify seagrass (Lee et al., 1998; Traganos and Reinartz, 2018a). Based on this, bottom-reflectance HSV parameters could be calculated. Including the mentioned features into the training model of the classifier yields the potential to make classes more distinguishable. Moreover, the integration of an object-based image analysis approach into the classification framework has been proven to be effective for seagrass mapping (Roelfsema et al., 2014).

5.2.3 Seagrass Extent

As shown in Figure 19 A1, the classification model GeoSplit 2 Spectral Range 2 (minimum extent) manages to map seagrass between complex ripples well, but fails to identify the clearly visible meadow in the north-west. The shallow water seagrass of Figure 19 B1 shows a similar extent to the one mapped by ClassBased Spectral Range 2 (Figure 19 B2) and underestimates areas around 26°N, 78°W. However, it classifies most of the dark area in the north as seagrass as well, which is likely to not be seagrass (Allen Coral Atlas, 2020; The Nature Conservancy, 2019). The Bahamas wide minimum seagrass extent (Figure 18) seems to underestimate large areas with depth of more than 3 m in the south and east. This underestimation is likely caused by the classification model's setup. The used geographical split causes the classifier to be trained on narrowly distributed data in the south, therefore, lacking the spatial variability needed for a complex and vast study area like the Bahamas. Moreover, ground truth data is mostly taken from near-shore areas, feeding into the problem of lacking spatial variability and causing the classifier to manly detect shallow water seagrass. This is supported by the probability map of GeoSplit 2 Spectral Range 2 (Figure 18 1A), which indicates that the classifier identified weak spectral ranges of seagrass within the aforementioned areas. The aforementioned misclassification of seagrass with other bottom features is likely caused by the lack of spatial variability in the Non-Seagrass ground TD, causing the classifier to not have enough data to distinguish between the present bottom classes.

The extent mapped using ClassBased Spectral Range 2 (maximum extent) shows a precise identification of the seagrass meadow in the north-west of Figure 19 A2, which was not detected with GeoSplit 2 Spectral Range 2. It also classified the meadows between and close to the ripples correctly, without underestimating them. Figure 19 B2 shows the same underestimation as the minimum extent in the north-east but no strong overestimation in the north. The reason for the overall larger seagrass extent classified with ClassBased Spectral Range 2 is the strong spatial variability of the TD, since it covers both shallow and deeper water seagrass distributed over the whole Bahamian carbonate platforms.

Both estimates show unnatural seagrass meadow borders in the south (Figure 18), which can be traced back to the aforementioned pre-processing challenges around tile edges (Chapter 5.1.1). The visual assessment of the minimum and maximum extent shows a higher probability for the maximum extent to represent the true extent of the Bahamian seagrasses.

The mapped seagrass extent shows an underestimation of dense, and especially sparse seagrass,

which is supported by the accuracy assessment in Chapter 5.2.4 (C. Roelfsema, personal communication; 29.07.2021). A reason for the underestimation of sparse seagrass is that it causes mixed pixels of seagrass and sand at the 10 m resolution of Sentinel-2, and that the classifier was trained on dense seagrass data only. In order to detect small patches of seagrass, imagery with a spatial resolution smaller than the 10 m would be necessary. A possible way to work around the sparse seagrass challenge could be a division approach and therefore the creation of different threshold probability ranges for seagrass. This would account for different cover types since the probability of a pixel refers to the pureness of its seagrass spectral content. Roelfsema et al. (2009) classified four different seagrass cover levels (1-25%, 25-50%, 50-75% and 75-100%), while Lyons et al. (2013) identified three (1-40%, 40-70% and 70-100%). Within the Wider Caribbean region, Webnitz 2008 classified three cover levels (<30%, 30-70% and 70-100%). The introduction of a division approach would also benefit the accuracy of estimated carbon stocks and will be discussed further in Chapter 5.3.1.

Figure 20 shows boxplots for the classified Seagrass and Non-Seagrass classes, with minimal overlaps of interquartile ranges for both frameworks of the minimum and maximum extent (ClassBased Spectral Range 2 and GeoSplit Spectral Range 2). This implies a strong separability between both classes, supporting the effectivity of the used frameworks and TD (Figure 16).

A visual comparison of the maximum mapped area with the ACA classified area (Figure 18, Figure 19) shows that both approaches identify seagrass in similar areas, but with different extents. As shown in Figure 19 A3, the ACA seagrass extent covers most of the meadows between the ripples and the one in the north-west but its borders do not follow the meadow borders. A reason for this could be the used Planet imagery, which shows low signal-to-noise ratios over nearshore waters causing a decline of image quality (Traganos et al., 2017). This underlines the suitability of Sentinel-2 for seagrass mapping, despite its coarser resolution.

As mentioned in Chapter 2.1, seagrass can be easily confused with algae due to their similar appearance (Seagrasswatch, 2021). However, a visual assessment of the mapped extents does not show a noticeable misclassification. A reason for this could be the minimisation of algae-dense images through pre-processing, even though the 20^{th} percentile approach selects darker pixels which could represent algae. Moreover, the classification seems to have been strictly trained on seagrass. The seasonal nature of growth and disappearance of algae blooms combined with a multi-temporal approach causes them to have less clear borders than seagrass meadows, which makes them easier to be distinguished visually (D'Silva et al., 2012). In order to utilise this effect within the classi-

fication framework, an object-based approach should be implemented. The aforementioned cloud shadow artifacts only caused minimal misclassifcations.

5.2.4 Accuracy Assessment

Even though both generated maps achieved acceptable OAs (77.60 and 72.20%), this does not reflect the accuracy of the single classes (Finegold and Ortmann, 2016). The high UA scores of 83.65 and 87.75% indicate that most of the classified seagrass area matches the VD and therefore the ground truth data. The lower PA scores of 68.60 and 51.60% indicate that a large area was missed by the classification (Sari et al., 2021). This suggests a general underestimation pattern by both classification models, which is supported by the findings of Chapter 5.2.3. The model GeoSplit 2 Spectral Range 2 shows a higher F1-score than the ClassBased Spectral Range 2 (75.3 and 64.99%, respectively), indicating a statistically better seagrass classification when based on ground truth data. A reason for this could be the stronger separability of classes within the TD (Figure 16). As suggested in Chapter 5.2.2, the spatial variability of the ACA classified data could require an increased number of TD points to cover as much of the seagrass spectral range as possible. However, both classification frameworks show a similar inter-class separability within the classified product (Figure 20).

A comparison between accuracies of this work and the ACA classification could not be performed since the ACA has not published Bahama-specific accuracies. Using Landsat sensors of coarser resolution than Sentinel-2, Wabnitz et al. (2008) achieved OAs of 71.80 and 63.30% for Lee Stocking Island and East Andros, respectively. This, combined with UA and PA values of under 50% for both regions suggest a better suitability of Sentinel-2 for seagrass mapping. However, these values only represent segments of The Bahamas, and do not merely depend on the used sensor but also on the classification framework.

5.2.5 Seagrass Area Literature Comparison

The seagrass extent mapped in this thesis equals about 3.4 to 7.9% of the global area identified by Green and Short (2003). Compared to already existing seagrass extent maps for Bahamian waters, this thesis classified the smallest area. It covers between 18 to 42.22% of the area of Wabnitz et al. (2008), 20.70 to 48.53% of the area mapped by the Nature Conservancy, and 25.29 to 59.31% of the area identified by the ACA (The Nature Conservancy, 2019; Allen Coral Atlas, 2020). The

reason for these differences could be a combination of the missed sparse seagrass area (Chapter 5.2.3) and an overestimation by the other mapping efforts due to the use of different imagery and mapping procedures.

Wabnitz et al. (2008) used Landsat imagery with a spatial resolution of 30 m as a base for the classification, which increases the probability for mixed pixels and, therefore, misclassification. The Nature Conservancy and ACA ran classifications on Planet Dove imagery, which shows low signal-to-noise ratios and could be susceptible to misclassification (The Nature Conservancy, 2019; Allen Coral Atlas, 2020; Traganos et al., 2017).

The high probability of missing sparse seagrass area creates a challenge when comparing different seagrass area extents. Even though the ACA project used sparse and dense seagrass ground truth data for the classification, both classes were merged to one Seagrass class for the classified map (Allen Coral Atlas, 2020; Lyons et al., 2020). Wabnitz et al. (2008) differentiated between cover levels within the classification procedure, but states seagrass area based on a merged class. Therefore, the two aforementioned classified extents are not suitable for area comparisons. The Nature Conservancy, on the other hand, states areas for sparse and dense seagrass. With a dense seagrass area of 14,900.20 km^2, the Nature Conservancy classified about 26.50% more than the minimum area and about half of the maximum extent mapped in this work (The Nature Conservancy, 2019). A visual comparison of the mapped maximum of this thesis with the map generated by the Nature Conservancy shows that most of the maximum seagrass extent is classified as sparse by the Nature Conservancy. This could be caused by the used probability threshold of 60% in this thesis while most other authors used probabilities over 70% to map dense seagrass (Roelfsema et al., 2009; Lyons et al., 2013; Wabnitz et al., 2008). Therefore, the use of a different threshold could make dense seagrass maps more comparable.

The generation of minimum and maximum seagrass extent maps with satisfying accuracies demonstrates the realisation of objective 2. Nonetheless, the input-data preparation and the differentiation between seagrass cover types have to be improved.

5.3 Carbon

The following chapters will analyse the Bahamian seagrass carbon stock and sequestration potential regarding data uncertainties and climate change implications.

5.3.1 Carbon Stocks

The base for Tier 1 carbon stock ranges (Chapter 4.1.1) are global averages which cause low accuracies when used for country-specific calculations. The error estimated for the AGB range is +/-50% and +/-90% for soil carbon pools (The Blue Carbon Initiative, 2014). This is supported by the minimum carbon stock of Tier 1 being 17 times smaller, and the maximum stock being 5 times larger than the Tier 2 stocks. Therefore, it is necessary to create region-specific ranges.

The uncertainties of Tier 2 estimations can be divided into two categories: calculation-based and biological-based. A calculation-based uncertainty lies within Equation 3, which is a simplification of the AGB:BGB-ratio variability of different species (Duarte and Chiscano, 1999). However, species-specific ratios are not always available and its inclusion into calculations would not be cost beneficial. Basing biomass carbon stock ranges on the proportions of species in relation to seagrass area is favourable if the total seagrass extent was mapped. However, since the mapped Bahamian seagrass extent is likely to only cover dense species, it would be sensible to adjust the calculations accordingly. The division of cover classes based on probabilities, as described in Chapter 5.2.3, could be combined with more species-specific in-situ data to create more accurate carbon stock ranges. The use of bio-regional soil carbon was necessary due to the lack of country-specific data, but introduces another source of uncertainty. This uncertainty has the highest influence on carbon stock ranges since soil carbon represents the largest part of the total stock (Fourqurean et al., 2012).

Biological-based uncertainties include inter-annual productivity variations, causing most in-situ data samples to not reflect averaged values (van Tussenbroek et al., 2014). Moreover, sampling sites can vary in depth, influencing seagrass carbon storage capacity due to reduced photosynthesis (Duarte, 1991; Serrano et al., 2014). Therefore, depth-dependent seagrass area classifications could help to create more precise carbon stock estimations. Another factor of uncertainty is allochthonous carbon, which influences the sediment carbon of samples taken from seagrass areas within close proximity to other marine ecosystems (Kennedy et al., 2010; Santos et al., 2021). This causes these samples to not be representative for the seagrass ecosystem. However, few pa-

pers state neighbouring ecosystems and the possibility for allochtonous carbon.

Based on the Tier 2 assessment, Bahamian seagrass could store between 4.32 and 10.85% of the minimum, and 2.16 to 5.42% of maximum global carbon stock estimate (Fourqurean et al., 2012). Lovelock et al. (2017) estimates that about 50% of seagrass carbon is released within the first 10 years following meadow disturbance. If all Bahamian seagrass would be lost at once, it would therefore cause a release of 33,3254,503.35 to 835,860,597.92 Mg of CO_2 within one decade. This equals 0.92 to 2.29% of the global emissions of 2018, and 175 to 439 times the Bahamian emissions of the same year, underling the importance of conserving this ecosystem (Friedlingstein et al., 2020).

5.3.2 Carbon Sequestration Potential

As with carbon stock estimation (Chapter 5.3.1), the carbon sequestration potential of seagrass shows similar reasons for uncertainties. Sequestration rates are species and depth dependent and show inter-annual variability (Buchan, 2000; Serrano et al., 2014). The potentials of same species also depend on location. The dense species *Thalassia testudium* sequesters four times as much CO_2 per year when growing in Bahamian waters compared to Colombian waters (Dierssen et al., 2010; Serrano et al., 2021).

According to the carbon sequestration potentials of Chapter 4.4, Bahamian seagrass could account for 30.85 to 72.35% of the ecosystems yearly global sequestration rate (Fourqurean et al., 2012). Its ability to sequester 17 to 40 times the amount of carbon which was emitted by The Bahamas in 2018 suggests a carbon-positive state for The Bahamas (Friedlingstein et al., 2020). The loss of each square kilometre of seagrass equals a sequestration potential loss of 2,600 tonnes CO_2 per year.

The successful estimation of carbon stock ranges and sequestration potentials for the Bahamian seagrass ecosystem demonstrates the achievement of objective 3. However, it also underlines the need for country-specific soil carbon in-situ data.

5.4 Algorithm Scalability

Even though the use of Sentinel-2 has been proven suitable for seagrass mapping in The Bahamas, its coverage can cause complications when used in other countries. Sentinel-2 does not cover islands smaller than 100 km^2 outside of the Mediterranean, which represents problems for many Small Island Developing States like Mauritius. Its northern most islands, South Agalega Islands, feature coastal seagrass meadows, which cannot be mapped by the approach in this work due to the lack of Sentinel-2 imagery (Allen Coral Atlas, 2020). A possible solution for this could be the integration of additional satellite missions, which cover the aforementioned spatial gaps.

The pre-processing procedure for cloud reduction worked well, but needs improvement for tropical countries with higher cloud coverage. Even though the multi-temporal approach increases the probability to find cloud free images for the composite, the cloud coverage of some countries is too dense to create a useful image. Within the used years of 2017 to 2021, Sentinel-2 did not record cloud-free images for two thirds of Kiribati. The integration of additional satellite missions could also minimise this problem by increasing the revisiting frequency and therefore the chance of cloud-free imagery.

The scalability of the pre-processing procedure is limited when applied to study areas with strong turbidity, since the use of the 20^{th} percentile increases its visibility by only using darker pixels. Turbid waters are challenging for seagrass mapping (Chapter 2.4), creating the necessity to include a turbidity filter before the composite is built.

The used masking methods are designed to work in different regions of the world and the land masking accounts for two kinds of land surface. However, the correct identification of the surface type is necessary, and more complex ones might make the use of other sigma and sensitivity threshold values necessary (Chapter 3.3.4). The complexity of the Bahamian coastline already demonstrated a challenge for this masking method, and testing it on a variety of land surfaces and coastlines is necessary to evaluate the true scalability of the landmasking method. Both masking methods depend strongly on the manual placement of bounding boxes, which creates the opportunity to achieve strong separability between classes, but the correct placement of bounding boxes is also time intensive.

The scalability of the supervised classification depends strongly on the available country-specific data. If both ground truth and classified data are available, the GeoSplit and ClassBased classification models can be adjusted accordingly. The availability of only classified data would require the

introduction of a new classification framework, since the VD would have to be chosen differently, ideally from a dataset of higher accuracy than the TD.

The implementation of the pre-processing and classification workflow in GEE is essential for the scalability and replicability of this thesis. It is easily adjustable to different study areas, while allowing for effortless code sharing. Even though GEE can handle large amounts of data and performed well at pre-processing four years of Sentinel-2 imagery for the Bahamas, larger study areas like Mexico might require the segmentation of the Sentinel-2 pre-processing into smaller regions to not exceed GEEs computational power. However, this represents only a small downside compared to the benefits brought by the use of this cloud computing platform.

The aforementioned aspects demonstrate a generally good scalability of the used algorithms but underline the complications which can be brought about by more complex study regions and the lack of data.

5.5 Nationally Determined Contributions

The large amount of carbon stored in Bahamian seagrass meadows combined with their high CO_2 sequestration potential underlines the importance of this ecosystem and its relevance for Bahamian NDCs. With the potential to sequester 17 to 40 times the amount of CO_2 emitted by The Bahamas in 2018, seagrass contributes strongly to climate change mitigation actions.

Moreover, its large extent has a strong positive effect on climate change adaptation actions, since it purifies water, acts as a nursing ground for fish, and reduces the impacts of sea level rise, flooding and land erosion (Waycott et al., 2011; Green and Short, 2003; UNEP, 2020a; Twomey et al., 2020).

Even though Bahamian seagrass is essential for the country's climate change mitigation and adaptation actions, only 6 to 11 % of its area lies within MPAs. This shows that the focus of Bahamian MPA design lied within other ecosystems. However, in order to preserve the country's carbon stock, sequestration rate, and other ecosystem services, seagrass needs to be higher prioritised in terms of conservation.

6 Conclusion

The aim of this thesis was to design scalable algorithms within the cloud computing platform GEE to create country-specific multi-temporal Sentinel-2 composites, seagrass maps, and carbon inventories for the ten countries which currently recognise seagrass within their NDCs. Due to the limited availability of reference data, only Bahamian seagrass was classified, and its carbon stock and sequestration potential estimated.

The developed pre-processing algorithms include environmental noise filtering and land and optically deep water masking. Six classification models were designed based on ground truth and classified data provided by the ACA. In-situ carbon data was acquired through an intensive literature review.

Based on the two classification models with the highest seagrass F1-score at 60% probability, Bahamian seagrass covers an area of 11,779.44 km^2 and the maximum 27,629.32 km^2. The accuracy assessment analysis shows an underestimation of the mapped seagrass area, while the visual map assessment indicates that only dense meadows were classified. Classification uncertainties lie within the used composite and the original resolution of TD and VD. The composite shows insufficient data at tile edges, and the resolution reduction of the reference data caused mixed pixels, which influences the classification. Compared to existing literature, the Bahamian seagrass extent mapped in this thesis represents the smallest area.

The mapped seagrass extent can store between 181,610,083.57 and 455,509,862.63 Mg carbon, and has the potential to sequester 31.02 to 72.75 Mt CO_2 per year. This sequestration rate equals 17 to 40 times the Bahamian emissions of 2018, leading to a carbon-neutral state. Uncertainties are brought about by the use of non-county-scale soil carbon data, calculation simplifications, and the general variability of seagrass carbon data depending on several environmental factors.

The designed pre-processing algorithms show a good scalability for countries of similar complexity to The Bahamas, but will reach limits when applied to larger study areas, regions with dense cloud coverage, or countries with challenging land surfaces types. Depending on the kind of data available for training and validation, the developed supervised classification models have to be adjusted. Even though GEE has its limits when handling large amounts of data, it is an essential and powerful tool for the creation of scalable and replicable workflows which allow for easy adaptability.

The generated seagrass distribution maps, associated carbon stocks, and sequestration potentials highlight the importance of Bahamian seagrass for climate change adaptation and mitigation actions, and therefore for the inclusion into the NDCs of the Paris Agreement. In order to preserve seagrass ecosystem services, Bahamian authorities need to conserve and restore this habitat. Moreover, these data inventories yield the potential to support management efforts in terms of necessary MPA development, as well as interdisciplinary scientific research in terms of biodiversity hotspot identification.

The approaches developed in this thesis can contribute towards global seagrass carbon mapping, while demonstrating the need for refined pre-processing techniques, and country-specific ground truth and in-situ data.

List of Figures

List of Tables

ACRONYMS

ACA Allen Coral Atlas

AGB Above-Ground Biomass

BGB Below-Ground Biomass

C Carbon

EEZ Exclusive Economic Zones

ESA European Space Agency

FAO Food and Agriculture Organization of the United Nations

GAUL Global Administrative Unit Layers

GEE Google Earth Engine

H Hue

IPCC Intergovernmental Panel on Climate Change

LiDAR Light Detection and Ranging

MNDWI Modified Normalised Difference Water Index

MPA Marine Protected Area

NDC Nationally Determined Contributions

NOAA National Oceanic and Atmospheric Administration

OA Overall Accuracy

PA User's Accuracy

ROI Region of Interest

S Saturation

$\boldsymbol{R}_{hown}$ Water Leaving Reflectance

$\boldsymbol{R_{rs}}$ Above-Surface Remote Sensing Reflectance

$\boldsymbol{r_{rs}}$ Sub-Surface Remote Sensing Reflectance

TD Training Data

UA Producer's Accuracy

UNFCCC United Nations Framework Convention on Climate Change

UTM Universal Transverse Mercator

V Value

VD Validation Data

WGS84 World Geodetic System 1984

References

Åhlén, J., Bengtsson, E. and Lindell, T. (2003). Color Correction of Underwater Images Based on Estimation of Diffuse Attenuation Coefficients, *Proceedings of the PICS 2003: The PICS Conference, An International Technical Conference on The Science and Systems of Digital Photography, including the Fifth International Symposium on Multispectral Color Science* pp. 325–329.

Alkhatlan, A., Bannari, A., Ali, T. S., Abahussain, A. and Hameid, N. (2019). Mapping Submerged Aquatic Vegetation in Shallow Water of Arabian Gulf Using Water Spectral Indices, Field Observations and Landsat-OLI Data, *IGARSS 2019 - 2019 IEEE International Geoscience and Remote Sensing Symposium* pp. 302–305. DOI: 10.1109/IGARSS.2019.8898883.

Allen Coral Atlas (2020). Imagery, maps and monitoring of the world's tropical coral reefs. DOI: 10.5281/zenodo.3833246.
URL: *https://allencoralatlas.org/atlas/*

Alongi, D. M. (2018). *Blue Carbon: Coastal Sequestration for Climate Change Mitigation*, Springer International Publishing, Cham. DOI: 10.1007/978-3-319-91698-9.

Amani, M., Mahdavi, S., Afshar, M., Brisco, B., Huang, W., Mohammad Javad Mirzadeh, S., White, L., Banks, S., Montgomery, J. and Hopkinson, C. (2019). Canadian Wetland Inventory using Google Earth Engine: The First Map and Preliminary Results, *Remote Sensing* **11**(7): 842. DOI: 10.3390/rs11070842.

Bandeira, S. O. (1997). Dynamics, biomass and total rhizome length of the seagrass Thalassodendron ciliatum at Inhaca Island, Mozambique, *Plant Ecology* (130): 133–131.

Brando, V. E. and Dekker, A. G. (2003). Satellite hyperspectral remote sensing for estimating estuarine and coastal water quality, *IEEE Transactions on Geoscience and Remote Sensing* **41**(6): 1378–1387. DOI: 10.1109/TGRS.2003.812907.

Breiman, L. (2001). Random Forests, *Machine Learning* **45**(1): 5–32. DOI: 10.1023/A:1010933404324.
URL: *https://link.springer.com/content/pdf/10.1023/A:1010933404324.pdf*

Brodie, G., Holland, E., N'Yeurt, A. D. R., Soapi, K. and Hills, J. (2020). Seagrasses and seagrass habitats in Pacific small island developing states: Potential loss of benefits via human disturbance and climate change, *Marine pollution bulletin* **160**. DOI: 10.1016/j.marpolbul.2020.111573.

Buchan, K. C. (2000). The Bahamas, *Marine pollution bulletin* (41): 94–111.

ChartsBin (2010). Length of Coastline by Country. Accessed on 21.06.2021.
URL: *http://chartsbin.com/view/ofv*

Cullen-Unsworth, L. and Unsworth, R. (2013). Seagrass Meadows, Ecosystem Services, and Sustainability, *Environment: Science and Policy for Sustainable Development* **55**(3): 14–28. DOI: 10.1080/00139157.2013.785864.

den Hartog, C. and Kuo, J. (2006). Taxonomy and Biogeography of Seagrasses, *Seagrasses: Biology, Ecology and Conservation*, Springer, pp. 1–23. DOI: 10.1007/978-1-4020-2983-7_1.

Dierssen, H. M., Zimmerman, R. C., La Drake and Burdige, D. (2010). Benthic ecology from space: optics and net primary production in seagrass and benthic algae across the Great Bahama Bank, *Marine Ecology Progress Series* **411**: 1–15. DOI: 10.3354/meps08665.

Donchyts, G., Schellekens, J., Winsemius, H., Eisemann, E. and van de Giesen, N. (2016). A 30 m Resolution Surface Water Mask Including Estimation of Positional and Thematic Differences Using Landsat 8, SRTM and OpenStreetMap: A Case Study in the Murray-Darling Basin, Australia, *Remote Sensing* **8**(5). DOI: 10.3390/rs8050386.

Dörnhöfer, K., Göritz, A., Gege, P., Pflug, B. and Oppelt, N. (2016). Water Constituents and Water Depth Retrieval from Sentinel-2A—A First Evaluation in an Oligotrophic Lake, *Remote Sensing* **8**(11). DOI: 10.3390/rs8110941.

D'Silva, M. S., Anil, A. C., Naik, R. K. and D'Costa, P. M. (2012). Algal blooms: a perspective from the coasts of India, *Natural Hazards* **63**(2): 1225–1253. DOI: 10.1007/s11069-012-0190-9.

Duarte, C. M. (1991). Seagrass depth limits, *Aquatic Botany* **40**(4): 363–377. DOI: 10.1016/0304-3770(91)90081-F.

Duarte, C. M. and Chiscano, C. L. (1999). Seagrass biomass and production: a reassessment, *Aquatic Botany* **65**(1-4): 159–174. DOI: 10.1016/S0304-3770(99)00038-8.

Duarte, C. M., Kennedy, H., Marbà, N. and Hendriks, I. (2013a). Assessing the capacity of seagrass meadows for carbon burial: Current limitations and future strategies, *Ocean & Coastal Management* **83**: 32–38. DOI: 10.1016/j.ocecoaman.2011.09.001.

Duarte, C. M., Losada, I. J., Hendriks, I. E., Mazarrasa, I. and Marbà, N. (2013b). The role of coastal plant communities for climate change mitigation and adaptation, *Nature Climate Change* **3**(11): 961–968. DOI: 10.1038/nclimate1970.

Duarte, C. M., Middelburg, J. J. and Caraco, N. (2005). Major role of marine vegetation on the oceanic carbon cycle, *Biogeosciences* **2**(1): 1–8. DOI: 10.5194/bg-2-1-2005.

ESA (2015). *Sentinel-2 User Handbook*.

ESA (2020). Sentinel-2 Inforgraphic.

ESA (2021). Sentinel-2 L2A Data Quality Report Issue 40.

FAO UN (2014). Global Administrative Unit Layers 2015, Country Boundaries.

Feyisa, G. L., Meilby, H., Fensholt, R. and Proud, S. R. (2014). Automated Water Extraction Index: A new technique for surface water mapping using Landsat imagery, *Remote Sensing of Environment* **140**: 23–35. DOI: 10.1016/j.rse.2013.08.029.

Finegold, Y. and Ortmann, A. (2016). *Map Accuracy Assessment and Area Estimation: A Practical Guide*, FAO, Rome, Italy.

Flanders Marine Institute (2019). Maritime Boundaries Geodatabase: Maritime Boundaries and Exclusive Economic Zones (200NM). Accessed on 03.02.2021.
URL: *https://www.marineregions.org/*

Fonseca, M. S. and Cahalan, J. A. (1992). A preliminary evaluation of wave attenuation by four species of seagrass, *Estuarine, Coastal and Shelf Science* **35**(6): 565–576. DOI: 10.1016/S0272-7714(05)80039-3.

Fourqurean, J. W., Duarte, C. M., Kennedy, H., Marbà, N., Holmer, M., Mateo, M. A., Apostolaki, E. T., Kendrick, G. A., Krause-Jensen, D., McGlathery, K. J. and Serrano, O. (2012). Seagrass ecosystems as a globally significant carbon stock, *Nature Geoscience* **5**(7): 505–509. DOI: 10.1038/ngeo1477.

Friedlingstein, P., O'Sullivan, M., Jones, M. W., Andrew, R. M., Hauck, J., Olsen, A., Peters, G. P., Peters, W., Pongratz, J., Sitch, S., Le Quéré, C., Canadell, J. G., Ciais, P., Jackson, R. B., Alin, S., Aragão, Luiz E. O. C., Arneth, A., Arora, V., Bates, N. R., Becker, M., Benoit-Cattin, A., Bittig, H. C., Bopp, L., Bultan, S., Chandra, N., Chevallier, F., Chini, L. P., Evans, W., Florentie, L., Forster, P. M., Gasser, T., Gehlen, M., Gilfillan, D., Gkritzalis, T., Gregor, L., Gruber, N., Harris, I., Hartung, K., Haverd, V., Houghton, R. A., Ilyina, T., Jain, A. K., Joetzjer, E., Kadono, K., Kato, E., Kitidis, V., Korsbakken, J. I., Landschützer, P., Lefèvre, N., Lenton, A., Lienert, S., Liu, Z., Lombardozzi, D., Marland, G., Metzl, N., Munro, D. R., Nabel, Julia E. M. S., Nakaoka, S.-I., Niwa, Y., O'Brien, K., Ono, T., Palmer, P. I., Pierrot, D., Poulter, B., Resplandy, L., Robertson, E., Rödenbeck, C., Schwinger, J., Séférian, R., Skjelvan, I., Smith, A. J. P., Sutton, A. J., Tanhua, T., Tans, P. P., Tian, H., Tilbrook, B., van der Werf, G., Vuichard, N., Walker, A. P., Wanninkhof, R., Watson, A. J., Willis, D., Wiltshire, A. J., Yuan, W., Yue, X. and Zaehle, S. (2020). Global Carbon Budget 2020, *Earth System Science Data* **12**(4): 3269–3340. DOI: 10.5194/essd-12-3269-2020.

GEE (n.d.a). Sentinel-2: Cloud Probability. Accessed on 26.06.2021.
URL: *https://developers.google.com/earth-engine/datasets/catalog/COPERNICUS_S2_CLOUD_PROBABILITY*

GEE (n.d.b). Sentinel-2 MSI: MultiSpectral Instrument, Level-2A. Accessed on 26.06.2021.
URL: *https://developers.google.com/earth-engine/datasets/catalog/COPERNICUS_S2_SR*

Giardino, C., Bresciani, M., Valentini, E., Gasperini, L., Bolpagni, R. and Brando, V. E. (2015). Airborne hyperspectral data to assess suspended particulate matter and aquatic vegetation in a shallow and turbid lake, *Remote Sensing of Environment* **157**: 48–57. DOI: 10.1016/j.rse.2014.04.034.

Gorelick, N., Hancher, M., Dixon, M., Ilyushchenko, S., Thau, D. and Moore, R. (2017). Google Earth Engine: Planetary-scale geospatial analysis for everyone, *Remote Sensing of Environment* **202**: 18–27. DOI: 10.1016/j.rse.2017.06.031.

Grech, A., Chartrand-Miller, K., Erftemeijer, P., Fonseca, M., McKenzie, L., Rasheed, M., Taylor, H. and Coles, R. (2012). A comparison of threats, vulnerabilities and management approaches in global seagrass bioregions, *Environmental Research Letters* **7**. DOI: 10.1088/1748-9326/7/2/024006.

Green, E. P. and Short, F. T. (2003). *World atlas of seagrasses*, University of California Press. DOI: 10.1515/BOT.2004.029.

Hassanein, M., Lari, Z. and El-Sheimy, N. (2018). A New Vegetation Segmentation Approach for Cropped Fields Based on Threshold Detection from Hue Histograms, *Sensors (Basel, Switzerland)* **18**(4).

Hedley, J., Russell, B., Randolph, K. and Dierssen, H. (2016). A physics-based method for the remote sensing of seagrasses, *Remote Sensing of Environment* **174**: 134–147. DOI: 10.1016/j.rse.2015.12.001.

Hemminga, M. A. and Duarte, C. M. (2000). *Seagrass Ecology*, Cambridge University Press, Cambridge, United Kingdom.

Hird, J., DeLancey, E., McDermid, G. and Kariyeva, J. (2017). Google Earth Engine, Open-Access Satellite Data, and Machine Learning in Support of Large-Area Probabilistic Wetland Mapping, *Remote Sensing* **9**(12). DOI: 10.3390/rs9121315.

Hossain, M. S., Bujang, J. S., Zakaria, M. H. and Hashim, M. (2015). The application of remote sensing to seagrass ecosystems: an overview and future research prospects, *International Journal of Remote Sensing* **36**(1): 61–114. DOI: 10.1080/01431161.2014.990649.

IPCC (2014). *2013 Supplement to the 2006 IPCC Guidelines for National Greenhouse Gas Inventories: Wetlands*, IPCC, Switzerland.

IPCC (2021). *Summary for Policymakers: Climate Change 2021: The Physical Science Basis. Contribution of Working Group I to the Sixth Assessment Report of the Intergovernmental Panel on Climate Change*, Cambridge University Press.

Juel, A., Groom, G. B., Svenning, J.-C. and Ejrnæs, R. (2015). Spatial application of Random Forest models for fine-scale coastal vegetation classification using object based analysis of aerial orthophoto and DEM data, *International Journal of Applied Earth Observation and Geoinformation* **42**: 106–114. DOI: 10.1016/j.jag.2015.05.008.

Kay, S., Hedley, J. and Lavender, S. (2009). Sun Glint Correction of High and Low Spatial Resolution Images of Aquatic Scenes: a Review of Methods for Visible and Near-Infrared Wavelengths, *Remote Sensing* **1**(4): 697–730. DOI: 10.3390/rs1040697.

Kennedy, H., Beggins, J., Duarte, C. M., Fourqurean, J. W., Holmer, M., Marbà, N. and Middelburg, J. J. (2010). Seagrass sediments as a global carbon sink: Isotopic constraints, *Global Biogeochemical Cycles* **24**(4). DOI: 10.1029/2010GB003848.

Keshava, N. (2003). A Survey of Spectral Unmixing Algorithms, *Lincoln Laboratory Journal* **14**(1).

Kirk, J. T. (1977). Attenuation of light in natural waters, *Marine and Freshwater Research* **28**(4). DOI: 10.1071/mf9770497.

Komatsu, T., Hashim, M., Nurdin, N., Noiraksar, T., Prathep, A., Stankovic, M., Tong, P. H. S., Pham, M. T., van Cao, L., Sam, W., Phauk, S., Muslim, A. M., Yahya, N. N., Terauchi, G., Sagawa, T. and Hayashizaki, K.-i. (2020). Practical mapping methods of seagrass beds by satellite remote sensing and ground truthing, *Coastal Marine Science* **43**(1).

Landfall (2021). Explorer Chart: Bahamas. Accessed on 06.08.2021.
URL: *https://www.landfallnavigation.com/explorer-charts-bahamas-turks-caicos.html#reviewformwrap*

Lee, K.-S., Park, S. R. and Kim, Y. K. (2007). Effects of irradiance, temperature, and nutrients on growth dynamics of seagrasses: A review, *Journal of Experimental Marine Biology and Ecology* **350**(1-2): 144–175. DOI: 10.1016/j.jembe.2007.06.016.

Lee, Z., Carder, K. L., Mobley, C. D., Steward, R. G. and Patch, J. S. (1998). Hyperspectral remote sensing for shallow waters. I. A semianalytical model, *Applied optics* **37**(27): 6329–6338. DOI: 10.1364/AO.37.006329.

Lee, Z., Carder, K. L., Mobley, C. D., Steward, R. G. and Patch, J. S. (1999). Hyperspectral remote sensing for shallow waters. 2. Deriving bottom depths and water properties by optimization, *Applied optics* **38**(18): 3831–3843. DOI: 10.1364/ao.38.003831.

Li, R., Liu, J.-K., Sukcharoenpong, A., Yuan, J., Zhu, H. and Zhang, S. (2012). A Systematic Approach toward Detection of Seagrass Patches from Hyperspectral Imagery, *Marine Geodesy* **35**(3): 271–286. DOI: 10.1080/01490419.2012.699019.

Lovelock, C. E., Fourqurean, J. W. and Morris, J. T. (2017). Modeled CO2 Emissions from Coastal Wetland Transitions to Other Land Uses: Tidal Marshes, Mangrove Forests, and Seagrass Beds, *Frontiers in Marine Science* **4**. DOI: 10.3389/fmars.2017.00143.

Lyons, M. B., Roelfsema, C. M., Kennedy, E. V., Kovacs, E. M., Borrego-Acevedo, R., Markey, K., Roe, M., Yuwono, D. M., Harris, D. L., Phinn, S. R., Asner, G. P., Li, J., Knapp, D. E., Fabina, N. S., Larsen, K., Traganos, D. and Murray, N. J. (2020). Mapping the world's coral reefs using a global multiscale earth observation framework, *Remote Sensing in Ecology and Conservation* **6**(4): 557–568. DOI: 10.1002/rse2.157.

Lyons, M. B., Roelfsema, C. M. and Phinn, S. R. (2013). Towards understanding temporal and spatial dynamics of seagrass landscapes using time-series remote sensing, *Estuarine, Coastal and Shelf Science* **120**: 42–53. DOI: 10.1016/j.ecss.2013.01.015.

Macreadie, P. I., Allen, K., Kelaher, B. P., Ralph, P. J. and Skilbeck, C. G. (2012). Paleoreconstruction of estuarine sediments reveal human–induced weakening of coastal carbon sinks, *Global Change Biology* **18**(3): 891–901.

Macreadie, P. I., Baird, M. E., Trevathan-Tackett, S. M., Larkum, A. W. D. and Ralph, P. J. (2014). Quantifying and modelling the carbon sequestration capacity of seagrass meadows–a critical assessment, *Marine pollution bulletin* **83**(2): 430–439. DOI: 10.1016/j.marpolbul.2013.07.038.

Macreadie, P. I., Trevathan-Tackett, S. M., Skilbeck, C. G., Sanderman, J., Curlevski, N., Jacobsen, G. and Seymour, J. R. (2015). Losses and recovery of organic carbon from a seagrass ecosystem following disturbance, *Proceedings. Biological sciences* **282**(1817): 20151537. DOI: 10.1098/rspb.2015.1537.

Manzello, D. P., Enochs, I. C., Gledhill, D. K. and Johns, E. M. (2012). Ocean Acidification Refugia of the Florida Reef Tract, *PloS one* **7**(7). DOI: 10.1371/journal.pone.0041715.g001.

McKenzie, L. J., Nordlund, L. M., Jones, B. L., Cullen-Unsworth, L. C., Roelfsema, C. and Unsworth, R. K. F. (2020). The global distribution of seagrass meadows, *Environmental Research Letters* **15**(7): 074041. DOI: 10.1088/1748-9326/ab7d06.

Mcleod, E., Chmura, G. L., Bouillon, S., Salm, R., Björk, M., Duarte, C. M., Lovelock, C. E., Schlesinger, W. H. and Silliman, B. R. (2011). A blueprint for blue carbon: toward an improved understanding of the role of vegetated coastal habitats in sequestering CO 2, *Frontiers in Ecology and the Environment* **9**(10): 552–560.

Millard, K. and Richardson, M. (2015). On the Importance of Training Data Sample Selection in

Random Forest Image Classification: A Case Study in Peatland Ecosystem Mapping, *Remote Sensing* **7**(7): 8489–8515. DOI: 10.3390/rs70708489.

Murray, N. J., Phinn, S. R., DeWitt, M., Ferrari, R., Johnston, R., Lyons, M. B., Clinton, N., Thau, D. and Fuller, R. A. (2019). The global distribution and trajectory of tidal flats, *Nature* **565**(7738): 222–225. DOI: 10.1038/s41586-018-0805-8.

Navarro, J. A. (2017). First Experiences with Google Earth Engine, *Proceedings of the 3rd International Conference on Geographical Information Systems Theory, Applications and Management (GISTAM2017)* pp. 250–255. DOI: 10.5220/0006352702500255.

NOAA National Geophysical Data Center (2009). *ETOPO1 1 Arc-Minute Global Relief Model*, NOAA National Centers for Environmental Information.

Otsu, N. (1979). A Threshold Selection Method from Gray-Level Histograms, *IEEE Transactions on Systems, Man, and Cybernetics* **9**(1): 62–66. DOI: 10.1109/TSMC.1979.4310076.

Pan, Z., Glennie, C., Fernandez-Diaz, J. C. and Starek, M. (2016). Comparison of bathymetry and seagrass mapping with hyperspectral imagery and airborne bathymetric lidar in a shallow estuarine environment, *International Journal of Remote Sensing* **37**(3): 516–536. DOI: 10.1080/01431161.2015.1131869.

Pendleton, L., Donato, D. C., Murray, B. C., Crooks, S., Jenkins, W. A., Sifleet, S., Craft, C., Fourqurean, J. W., Kauffman, J. B., Marbà, N., Megonigal, P., Pidgeon, E., Herr, D., Gordon, D. and Baldera, A. (2012). Estimating Global "Blue Carbon" Emissions from Conversion and Degradation of Vegetated Coastal Ecosystems, *PloS one* **7**(9). DOI: 10.1371/journal.pone.0043542.

Phinn, S., Roelfsema, C., Dekker, A., Brando, V. and Anstee, J. (2008). Mapping seagrass species, cover and biomass in shallow waters: An assessment of satellite multi-spectral and airborne hyper-spectral imaging systems in Moreton Bay (Australia), *Remote Sensing of Environment* **112**(8): 3413–3425. DOI: 10.1016/j.rse.2007.09.017.

Phinn, S., Roelfsema, C., Kovacs, E., Canto, R., Lyons, M., Saunders, M. and Maxwell, P. (2018). Mapping, Monitoring and Modelling Seagrass Using Remote Sensing Techniques, *in* A. W. D. Larkum, G. A. Kendrick and P. J. Ralph (eds), *Seagrasses of Australia*, Springer International Publishing, Cham, pp. 445–487. DOI: 10.1007/978-3-319-71354-0_15.

Potouroglou, M., Bull, J. C., Krauss, K. W., Kennedy, H. A., Fusi, M., Daffonchio, D., Mangora, M. M., Githaiga, M. N., Diele, K. and Huxham, M. (2017). Measuring the role of seagrasses in regulating sediment surface elevation, *Scientific reports* **7**(1). DOI: 10.1038/s41598-017-12354-y.

Rekik, A., Zribi, M., Benjelloun, M. and ben Hamida, A. (2006). A k-Means Clustering Algorithm Initialization for Unsupervised Statistical Satellite Image Segmentation, *1ST IEEE International Conference on E-Learning in Industrial Electronics* pp. 11–16. DOI: 10.1109/ICELIE.2006.347204.

Roelfsema, C., Kovacs, E. M., Saunders, M. I., Phinn, S., Lyons, M. and Maxwell, P. (2013). Challenges of remote sensing for quantifying changes in large complex seagrass environments, *Estuarine, Coastal and Shelf Science* **133**: 161–171. DOI: 10.1016/j.ecss.2013.08.026.

Roelfsema, C. M., Lyons, M., Kovacs, E. M., Maxwell, P., Saunders, M. I., Samper-Villarreal, J. and Phinn, S. R. (2014). Multi-temporal mapping of seagrass cover, species and biomass: A semi-automated object based image analysis approach, *Remote Sensing of Environment* **150**: 172–187. DOI: 10.1016/j.rse.2014.05.001.

Roelfsema, C. M., Phinn, S. R., Udy, N. and Maxwell, P. (2009). An integrated field and remote sensing approach for mapping Seagrass Cover, Moreton Bay, Australia, *Journal of Spatial Science* **54**(1): 45–62. DOI: 10.1080/14498596.2009.9635166.

Sagar, S., Brando, V. and Sambridge, M. (2014). Noise Estimation of Remote Sensing Reflectance Using a Segmentation Approach Suitable for Optically Shallow Waters, *IEEE Transactions on Geoscience and Remote Sensing* **52**(12): 7504–7512. DOI: 10.1109/TGRS.2014.2313129.

Santos, I. R., Burdige, D. J., Jennerjahn, T. C., Bouillon, S., Cabral, A., Serrano, O., Wernberg, T., Filbee-Dexter, K., Guimond, J. A. and Tamborski, J. J. (2021). The renaissance of Odum's outwelling hypothesis in 'Blue Carbon' science, *Estuarine, Coastal and Shelf Science* **255**. DOI: 10.1016/j.ecss.2021.107361.

Sari, I. L., Weston, C. J., Newnham, G. J. and Volkova, L. (2021). Assessing Accuracy of Land Cover Change Maps Derived from Automated Digital Processing and Visual Interpretation in Tropical Forests in Indonesia, *Remote Sensing* **13**(8): 1446. DOI: 10.3390/rs13081446.

Saunders, M. I., Leon, J., Phinn, S. R., Callaghan, D. P., O'Brien, K. R., Roelfsema, C. M., Lovelock, C. E., Lyons, M. B. and Mumby, P. J. (2013). Coastal retreat and improved water quality mitigate losses of seagrass from sea level rise, *Global change biology* **19**(8): 2569–2583. DOI: 10.1111/gcb.12218.

Seagrasswatch (2021). What is Seagrass. Accessed on 30.03.2021.
URL: *https://www.seagrasswatch.org/seagrass/*

Seddon, N., Daniels, E., Davis, R., Chausson, A., Harris, R., Hou-Jones, X., Huq, S., Kapos, V., Mace, G. M., Rizvi, A. R., Reid, H., Roe, D., Turner, B. and Wicander, S. (2020). Global recognition of the importance of nature-based solutions to the impacts of climate change, *Global Sustainability* **3**. DOI: 10.1017/sus.2020.8.

Serrano, O., Gómez-López, D. I., Sánchez-Valencia, L., Acosta-Chaparro, A., Navas-Camacho, R., González-Corredor, J., Salinas, C., Masque, P., Bernal, C. A. and Marbà, N. (2021). Seagrass blue carbon stocks and sequestration rates in the Colombian Caribbean, *Scientific reports* **11**(1): 11067. DOI: 10.1038/s41598-021-90544-5.

Serrano, O., Lavery, P. S., Rozaimi, M. and Mateo, M. Á. (2014). Influence of water depth on the carbon sequestration capacity of seagrasses, *Global Biogeochemical Cycles* **28**(9): 950–961. DOI: 10.1002/2014GB004872.

Shelestov, A., Lavreniuk, M., Kussul, N., Novikov, A. and Skakun, S. (2017). Exploring Google Earth Engine Platform for Big Data Processing: Classification of Multi-Temporal Satellite Imagery for Crop Mapping, *Frontiers in Earth Science* **5**. DOI: 10.3389/feart.2017.00017.

Short, F., Carruthers, T., Dennison, W. and Waycott, M. (2007). Global seagrass distribution and diversity: A bioregional model, *Journal of Experimental Marine Biology and Ecology* **350**(1-2): 3–20. DOI: 10.1016/j.jembe.2007.06.012.

Short, F., Polidoro, B., Livingstone, S. R., Carpenter, K. E., Bandeira, S., Bujang, J. S., Calumpong, H. P., Carruthers, T. J., Coles, R. G., Dennison, W. C., Erftemeijer, P. L., Fortes, M. D., Freeman, A. S., Jagtap, T. G., Kamal, A. H. M., Kendrick, G. A., Judson Kenworthy, W., La Nafie, Y. A., Nasution, I. M., Orth, R. J., Prathep, A., Sanciangco, J. C., van Tussenbroek, B., Vergara, S. G., Waycott, M. and Zieman, J. C. (2011). Extinction risk assessment of the world's seagrass species, *Biological Conservation* **144**(7): 1961–1971. DOI: 10.1016/j.biocon.2011.04.010.

Siikamäki, J., Sanchirico, J. N., Jardine, S., McLaughlin, D. and Morris, D. (2013). Blue Carbon: Coastal Ecosystems, Their Carbon Storage, and Potential for Reducing Emissions, *Environment: Science and Policy for Sustainable Development* **55**(6): 14–29. DOI: 10.1080/00139157.2013.843981.

Story, M. and Congalton, R. (1986). Accuracy assessment: a user's perspective, *Photogrammetric Engineering and Remote Sensing* .

Stumpf, R. P., Holderied, K. and Sinclair, M. (2003). Determination of water depth with high-resolution satellite imagery over variable bottom types, *Limnology and Oceanography* **48**(1part2): 547–556. DOI: 10.4319/LO.2003.48.1_PART_2.0547.

The Blue Carbon Initiative (2014). *Coastal Blue Carbon: Methods for assessing carbon stocks and emissions factors in mangroves, tidal salt marshes, and seagrasses meadows*, International Union for Conservation of Nature (IUCN).

The Government of the Bahamas (2015). *Intended Natinally Determined Contributions (INDC) under the United Nations Framework Convention On Climate Change (UNFCCC)*.

The Nature Conservancy (2019). Caribbean Science Atlas. Accessed on 22.08.2021.
URL: *https://caribbeanscienceatlas.tnc.org/*

Thomas, N., Pertiwi, A. P., Traganos, D., Lagomasino, D., Poursanidis, D., Moreno, S. and Fatoyinbo, L. (2021). Space–Borne Cloud–Native Satellite–Derived Bathymetry (SDB) Models Using ICESat–2 And Sentinel–2, *Geophysical Research Letters* **48**(6). DOI: 10.1029/2020GL092170.

Traganos, D., Aggarwal, B., Poursanidis, D., Topouzelis, K., Chrysoulakis, N. and Reinartz, P. (2018a). Towards Global-Scale Seagrass Mapping and Monitoring Using Sentinel-2 on Google Earth Engine: The Case Study of the Aegean and Ionian Seas, *Remote Sensing* **10**(8). DOI: 10.3390/rs10081227.

Traganos, D., Cerra, D. and Reinartz, P. (2017). Cubesat-Derived Detection of Seagrasses Using Planet Imagery Following Unmixing-Based Denoising: Is Small the Next Big?, *The International Archives of the Photogrammetry, Remote Sensing and Spatial Information Sciences* **XLII-1/W1**: 283–287. DOI: 10.5194/isprs-archives-XLII-1-W1-283-2017.

Traganos, D., Poursanidis, D., Aggarwal, B., Chrysoulakis, N. and Reinartz, P. (2018b). Estimating Satellite-Derived Bathymetry (SDB) with the Google Earth Engine and Sentinel-2, *Remote Sensing* **10**(6): 859. DOI: 10.3390/rs10060859.

Traganos, D., Putri Pertiwi, A., Lee, C. B., Blume, A., Poursanidis, D. and Shapiro, A. (2021). Serverless regional mapping of the extent, carbon stocks, water quality, and bathymetry of seagrasses in East Africa: Manuscript submitted for publication.

Traganos, D. and Reinartz, P. (2018a). Interannual Change Detection of Mediterranean Seagrasses Using RapidEye Image Time Series, *Frontiers in plant science* **9**. DOI: 10.3389/fpls.2018.00096.

Traganos, D. and Reinartz, P. (2018b). Machine learning-based retrieval of benthic reflectance and Posidonia oceanica seagrass extent using a semi-analytical inversion of Sentinel-2 satellite data, *International Journal of Remote Sensing* **39**(24): 9428–9452. DOI: 10.1080/01431161.2018.1519289.

Traganos, D. and Reinartz, P. (2018c). Mapping Mediterranean seagrasses with Sentinel-2 imagery, *Marine pollution bulletin* **134**: 197–209. DOI: 10.1016/j.marpolbul.2017.06.075.

Twomey, A. J., O'Brien, K. R., Callaghan, D. P. and Saunders, M. I. (2020). Synthesising wave attenuation for seagrass: Drag coefficient as a unifying indicator, *Marine pollution bulletin* **160**(111661). DOI: 10.1016/j.marpolbul.2020.111661.

UNEP (2006). *Marine and coastal ecosystems and human wellbeing: A synthesis report based on the findings of the Millennium Ecosystem Assessment*, Nairobi, Kenya.

UNEP (2020a). *Out of the blue: The value of seagrasses to the environment and to people*, UNEP, Nairobi.

UNEP (2020b). Seagrasses, the forgotten ecosystems, *Foresight: Early Warning, Emerging Issues and Futures* .

UNEP-WCMC (2021). Protected Area Profile for Bahamas from the World Database of Protected Areas, July 2021. Accessed on 29.07.2021.
URL: *www.protectedplanet.net*

UNEP-WCMC and Short, F. T. (2018). Global Distribution of Seagrasses (version 6.0). Sixth update to the data layer used in Green and Short (2003).

UNEP-WCMC and Short, F. T. (2021). Global distribution of seagrasses (version 7.1). Seventh update to the data layer used in Green and Short (2003). DOI: 10.34892/X6R3-D211.

UNFCCC (2016). *Report of the Conference of the Parties on its twenty-first session, held in Paris from 30 November to 11 December 2015*.

UNFCCC (n.d.a). COP 21. Accessed on 07.06.2021.
URL: *https://unfccc.int/process-and-meetings/conferences/past-conferences/paris-climate-change-conference-november-2015/cop-21*

UNFCCC (n.d.b). Key aspects of the Paris Agreement. Accessed on 07.06.2021.
URL: *https://cop23.unfccc.int/process-and-meetings/the-paris-agreement/the-paris-agreement/key-aspects-of-the-paris-agreement*

UNFCCC (n.d.c). Nationally Determined Contributions (NDCs). Accessed on 07.06.2021.
URL: *https://cop23.unfccc.int/process-and-meetings/the-paris-agreement/nationally-determined-contributions-ndcs/nationally-determined-contributions-ndcs#eq-1*

UNFCCC (n.d.d). Paris Agreement - Status of Ratification. Accessed on 07.06.2021.
URL: *https://cop23.unfccc.int/process/the-paris-agreement/status-of-ratification*

United Nations (2017). Factsheet: People and Oceans.

Unsworth, R. K., Nordlund, L. M. and Cullen-Unsworth, L. C. (2019). Seagrass meadows support global fisheries production, *Conservation Letters* **12**(1). DOI: 10.1111/conl.12566.

Valentine, J. F. and Heck, K. L. (1999). Sargass herbivory: evidence for the continured grazing of marine grasses, *Marine Ecology Press Series* **176**: 291–302.

van Tussenbroek, B. I., Cortés, J., Collin, R., Fonseca, A. C., Gayle, P. M. H., Guzmán, H. M., Jácome, G. E., Juman, R., Koltes, K. H., Oxenford, H. A., Rodríguez-Ramirez, A., Samper-Villarreal, J., Smith, S. R., Tschirky, J. J. and Weil, E. (2014). Caribbean-wide, long-term study of seagrass beds reveals local variations, shifts in community structure and occasional collapse, *PloS one* **9**(3). DOI: 10.1371/journal.pone.0090600.

Veettil, B. K., Ward, R. D., Lima, M. D. A. C., Stankovic, M., Hoai, P. N. and Quang, N. X. (2020). Opportunities for seagrass research derived from remote sensing: A review of current methods, *Ecological Indicators* **117**: 106560. DOI: 10.1016/j.ecolind.2020.106560.

Wabnitz, C. C., Andréfouët, S., Torres-Pulliza, D., Müller-Karger, F. E. and Kramer, P. A. (2008). Regional-scale seagrass habitat mapping in the Wider Caribbean region using Landsat sensors: Applications to conservation and ecology, *Remote Sensing of Environment* **112**(8): 3455–3467. DOI: 10.1016/j.rse.2008.01.020.

Waycott, M., Duarte, C. M., Carruthers, T. J. B., Orth, R. J., Dennison, W. C., Olyarnik, S., Calladine, A., Fourqurean, J. W., Heck, K. L., Hughes, A. R., Kendrick, G. A., Kenworthy, W. J., Short, F. T. and Williams, S. L. (2009). Accelerating loss of seagrasses across the globe threatens coastal ecosystems, *Proceedings of the National Academy of Sciences of the United States of America* **106**(30): 12377–12381. DOI: 10.1073/pnas.0905620106.

Waycott, M., McKenzie, L. J., Mellors, J., EllisonJoanna C, J. C., Sheaves, M. T., Collier, C., Schwarz, A.-M., Webb, A., E Johnson, J. and Payr, C. E. (2011). Vulnerability of mangroves, seagrasses and intertidal flats in the tropical Pacific to climate change, *in* J. D. Bell, J. E. Johnson and A. J. Hobday (eds), *Vulnerability of Tropical Pacific Fisheries and Aquaculture to Climate Change*, pp. 297–368.

Xu, H. (2006). Modification of normalised difference water index (NDWI) to enhance open water features in remotely sensed imagery, *International Journal of Remote Sensing* **27**(14): 3025–3033. DOI: 10.1080/01431160600589179.